MÄLARDALEN UNIVERSITY
SWEDEN

School of Innovation, Design and Engineering

BACHELOR THESIS IN
AERONAUTICAL ENGINEERING
15 CREDITS, BASIC LEVEL 300

Conceptual Design of a Supersonic Jet Engine

by

Joakim Kareliusson
Melker Nordqvist

Västerås, September 2014
Advisor at MDH: Konstantinos G. Kyprianidis
Examiner: Mirko Senkovski

Abstract

This thesis is a response to the request for proposal issued by a joint collaboration between the AIAA Foundation and ASME/IGTI as a student competition to design a new turbofan engine intended for a conceptual supersonic business jet expected to enter service in 2025. Due to the increasing competition in the aircraft industry and the more stringent environmental legislations the new engine is expected to provide a lower fuel burn than the current engine intended for the aircraft to increase the chances of commercial success.

The thesis has one main and one secondary objective, the main objective is to perform a preliminary design of a jet engine, complying with the specifications stated in the request for proposal. The secondary objective is to evaluate whether the knowledge gathered from the BSc program in aeronautical engineering at Mälardalen University is sufficient to perform this kind of study and to recommend courses for future students who wish to perform a similar project. Due to time restrictions a full conceptual design has not been performed and the work has mainly been focused on the thermodynamic and aerodynamic design phases.

The thermodynamic analysis and optimization has been carried out using the Numerical Propulsion System Simulation (NPSS) code, where the cycle parameters such as fan pressure ratio (FPR), overall pressure ratio (OPR), turbine inlet temperature (TIT) and bypass ratio (BPR) have been optimized for cycle overall efficiency. With the cycle selected, and the fluid properties at the different flow stations known, the component aerodynamic design, sizing and efficiency calculations were performed using MATLAB, with equations and formulas found in the open literature together with literature developed at Chalmers University of Technology in Gothenburg, Sweden. Furthermore a number of research papers have been used for various parts of the thesis. Several aspects of the turbomachinery components have been evaluated to assure satisfactory performance. The result is a two spool low bypass axial flow engine of similar dimensions as the current engine but with increased efficiencies. A weighted fuel flow comparison of the two engines at the key operating conditions shows a fuel burn improvement of 11,8% for the new engine.

The conclusions drawn by the authors on the secondary objective is that even though the knowledge might be slightly insufficient to undertake this type of task, with proper guidance and determination it’s certainly not impossible.

Sammanfattning

Detta examensarbete är ett bidrag till en studenttävling skapad genom ett samarbete mellan *the AIAA Foundation* och *ASME/IGTI* där en ny motor avsedd för en business jet med överljudsegenskaper som förväntas tas i bruk år 2025 efterfrågas. På grund av den ökande konkurrensen inom flygindustrin och de strängare miljökraven förväntas den nya motorn förbränna mindre bränsle än den nuvarande motorn avsedd för flygplanet och därmed öka chanserna på marknaden.

Arbetet har två syften, det första är att utföra en preliminär design av en jetmotor som uppfyller de krav som finns i specifikationen. Det andra är att utvärdera huruvida förkunskaperna från flygingenjörsprogrammet på Mälardalens högskola är tillräckliga för att utföra den här typen av arbete och att rekommendera kurser för framtida studenter som vill utföra ett liknande projekt. På grund av tidsbegränsningar har en full preliminär design inte utförts, utan arbetet har huvudsakligen fokuserats på den termodynamiska och aerodynamiska designen.

Den termodynamiska analysen och optimeringen har utförts med hjälp av programmet *the Numerical Propulsion System Simulation* (NPSS) där övergripande cykelparametrar så som *fan pressure ratio (FPR), overall pressure ratio (OPR), turbine inlet temperature (TIT) och bypass ratio (BPR)* har optimerats för höga verkningsgrader i motorn. Då den termodynamiska analysen och optimeringen färdigställts och egenskaperna för gasen vid de olika stationerna i motorn var kända, beräknades komponenternas aerodynamiska design, storlekar och effektiviteter i MATLAB med hjälp av formler och ekvationer från öppen litteratur tillsammans med material som tagits fram på Chalmers tekniska högskola i Göteborg. I övrigt har ett antal forskningsuppsatser använts till olika delar av arbetet. Flera aspekter har utvärderats för kompressorer och turbiner för att säkerställa fullgod prestanda. Resultatet är en tvåspolig låg-bypass axialmotor med liknande dimensioner som den nuvarande motorn men med ökade effektiviteter. En jämförelse av bränsleförbrukning över ett typiskt uppdrag visar en bränslebesparing på 11,8% för den nya motorn.

På arbetets andra syfte är det författarnas åsikt att även om förkunskaperna är aningen otillräckliga för den här typen av projekt, så är det med god handledning och en gedigen arbetsinsats definitivt ingen omöjlig uppgift.

Acknowledgements

We would like to thank Konstantinos Kyprianidis for proposing this thesis, guiding us through the process and always responding quickly to questions.

We also want to thank Mirko Senkovski for considering us when the thesis proposal came, as well as the other teachers involved with the aeronautical program.

Contents

List of Figures

List of Tables

Nomenclature

Parameter	Symbol	Units
Absolute Velocity	C	m/s
Angularity Coefficient	C_θ	
Aspect Ratio	AR	
Axial Mach number	M_{ax}	
Axial Velocity	C_a	m/s
Blade Stress Level	AN^2	$m^2 \cdot RPS^2$
Blade Velocity	U	m/s
Bypass Ratio	BPR	
Chord	c	
Convergent – Divergent	$con - di$	
Corrected mass flow	W_c	kg/s
Core Efficiency	η_{core}	
Entry into Service	EIS	
Fan Pressure Ratio	FPR	
Flow Coefficient	ϕ	
Fuel to Air Ratio	FAR	
Gross Thrust	FG	N
High Pressure Compressor	HPC	
High Pressure	HP	
High Pressure Turbine	HPT	
Inlet Guide Vane	IGV	
Intercompressor Duct	ICD	
Interturbine Duct	ITD	
Isentropic Efficiency	η_{is}	
Loss Coefficient for Stator Blades	λ_N	
Lower Heating Value	LHV	MJ/kg
Low Pressure	LP	

Low Pressure Turbine	LPT	
Mach number	M	
Mass flow	W	kg/s
Momentum Drag	FD	N
Net Thrust	FN	N
Nozzle Guide Vane	NGV	
Overall Efficiency	η_{ov}	
Overall Pressure Ratio	OPR	
Pitch	s	
Polytropic Efficiency	η_{poly}	
Pressure Loss Factor	PLF	
Pressure Recovery	PR	
Propulsive Efficiency	η_{prop}	
Relative Blade Mach number	M_{rel}	
Relative Velocity	V	m/s
Revolutions per Minutes	RPM	
Revolutions per Seconds	RPS	
Specific Fuel Consumption	SFC	
Specific Thrust	SFN	Ns/kg
Stage Load	ψ	
Static Pressure	P	Pa
Static Temperature	T	K
Thermal Efficiency	η_{th}	
Thrust Coefficient	CV	
Total Pressure	P_0	Pa
Total Temperature	T_0	K
Transfer Efficiency	η_{tran}	
Turbine Inlet Temperature	TIT	K
Water to Air Ratio	WAR	

1 Introduction

1.1 Problem area

The request for proposal is a joint AIAA Foundation and ASME/IGTI student design competition where a new turbofan engine for a conceptual supersonic business jet aircraft expected to enter service in 2025 is requested. It will be able to travel from North America to Europe and back again within one business day. It can cruise at Mach 1.15 over land without creating a sonic boom on the ground. Over water, it can cruise at Mach 1.5. Transonic cruise at Mach 0.98 should offer similar cost per distance to subsonic private jets. [1]

Today's aircraft industry is very competitive. The commercial success of an aircraft highly depends on its ability to provide light weight, low noise, competitive fuel consumption, and in the end lower operating costs and passenger fares. A contributing factor to achieve this is the engine design. Furthermore, due to the increase of the environmental concerns over the impact of the growing civil aviation, the emission legislations set by the International Civil Aviation Organization (ICAO) are becoming more stringent. The airlines need to continuously reduce their operating costs, which combined with stringent emission legislations introduces new challenges for the aero-engine industry: new engines need to be developed for low operating costs as well as reduced environmental impact. A reduction of fuel consumption, which is directly proportional to CO2 emissions, can be achieved primarily by increasing component efficiencies, increasing OPR and TIT reducing SFN and engine size and weight. A number of novel engine concepts addressing these issues have been proposed over the years, some of which will be presented briefly in chapter two of this thesis. Implementations of such concepts however, involve a great financial risk for the manufacturers [2]. In this thesis, a more conventional cycle is considered.

Engine development is a multidisciplinary process covering thermodynamics, aerodynamics and solid mechanics, where the requirements of one discipline may very well contradict the requirements of another, and trade-offs between performance, size, weight, and costs continuously need to be made.

Engine specifications are provided in the RFP, including thrust requirements, maximum dimensions etc. A generic model of a baseline engine is also provided. The new engine is expected to have improved fuel consumption and overall performance, thus increasing the chances of commercial success for the aircraft. The new engine has been given the designation **MJ – Haran S14**.

1.2 Aim and objectives

There is one primary objective and one secondary objective for this thesis. The primary is to carry out a preliminary design for an engine complying with the requirements specified in the RFP. This can be broken down in the following steps:

1. Model the baseline engine and perform a thermodynamic study of the cycle performance.
2. Optimize the engine cycle for low fuel consumption, and high cycle overall efficiency.
3. Carry out preliminary sizing, efficiency calculations and aerodynamic design for the main engine components.
4. Create a schematic design of the engine including dimensions.

The secondary objective is to evaluate if the knowledge acquired from the courses at the aeronautical program at MDH is sufficient to carry out a preliminary engine design process, and to recommend courses for future students who wish to perform a similar task.

1.3 Work scope and limitations

Due to time restrictions a full preliminary design has not been carried out in more detail. The mechanical design is limited to the disc design of the HPC and HPT. No other material choices have been made and hence no overall weight estimations.

1.4 Thesis outline

Chapter 2 contains a literature review where published literature regarding the problem areas of the thesis is discussed. It provides an overview of relevant past and current research on the topic.

Chapter 3 provides the methodology used to achieve the results of the thesis, it motivates why and how certain parameters are chosen. It also contains a description of the software used.

In chapter 4 the results of the simulations and choice of parameters is presented and discussed. Some comparisons to the baseline engine are also provided.

Chapter 5 concludes the thesis, looking back and evaluating the objectives. Recommendations for future work are also presented.

2 Literature review

A large number of research papers have been published regarding the aero engine industry over the years. In this chapter, a few of these regarding important aspects of the engine design process will be discussed.

2.1 Reducing fuel consumption

Today one major concern in the industry is producing engines with better fuel economy, partially to reduce the operating costs for the airlines leading to lower fares for paying passengers, but also to address today's environmental concerns. A few approaches to achieve this has been proposed.

A summary of some of the current research being done in the search for more fuel efficient engines is provided in [2]. The author starts by discussing the limitations of increasing OPR and TIT in order to increase thermal efficiency and reduce SFC, which has been the trend for conventional cores over the past decades. Increasing OPR further than current designs is limited by HPC delivery temperature at take-off. Increasing TIT is limited by the maximum HPT rotor temperatures at take-off and top of climb. The increase of cooling flows for this reason is also a limited strategy since this represent losses in the cycle and will eventually lead to a loss in thermal efficiency.

In [3] the authors investigate the benefits of introducing Intercooled and intercooled recuperated cores. An intercooled core can be designed for a significantly higher overall pressure ratio, with reduced cooling requirements, providing a higher thermal efficiency than could be practically achieved with a conventional core. In an intercooled recuperated core a high thermal efficiency can be achieved at a low overall pressure ratio. The use of a variable geometry auxiliary nozzle for the intercooled engine, and a variable geometry LPT for the intercooled recuperated engine is also evaluated, showing further benefits. The use of recuperation is also investigated in [4], where a recuperated engine for a UAV is compared to a conventional design. The novel engine is expected to maintain the same weight as the conventional engine and extend the mission endurance by 15%.

In [5], a geared open rotor configuration engine is compared to an ultra-high bypass geared turbofan engine, with focus on minimizing fuel consumption and hence engine emissions. The open rotor concept is not a new idea, it was evaluated in the 80's in several flight tests, but most of them never got past that phase and lately the concept has resurfaced. In an open rotor configuration the propulsive efficiency may be increased without increasing nacelle drag, and losses due to transfer efficiency are comparable to those of a turbofan. The results show that the open rotor engine is heavier but the reduced SFC and nacelle drag makes up for this and a mission fuel burn improvement of approximately 15% compared to the turbofan is presented.

In [2] the author concludes by highlighting the fact that even though research of more efficient engine concepts exists, the aero engine design industry is primarily driven by economic considerations. Introducing these novel concepts to the market involves an economical and technological risk, and whether the potential reduction in fuel consumption outweighs these risks remains to be seen.

2.2 Computer aided design

Over the years, computers have become an invaluable tool for engineering purposes. In [6] the authors discuss the impact computers have had on the industry during the 1980's. Since then the use of computers have increased exponentially and software is constantly being developed and updated.

The authors of [7] discuss the development of a multidisciplinary optimization code at the time being developed at NASA Lewis research center for the design of structural components, subsonic and supersonic aircraft configuration design and airbreathing propulsion engine design. The design tool can optimize a system which can be defined in terms of fifty optimization subproblems. The system first formulates the design as a nonlinear mathematical problem, and solves the resulting problem based on data from specified input files.

In [8] another piece of software is described, meant to be used in the preliminary design phase of gas turbines. The software was created to allow for a quick preliminary design process allowing the engine suppliers the ability to evaluate numerous concepts to fulfill the market requirements. The system is built upon three major features:

i. All major engine components and their interrelations are assessed.
ii. Several relevant disciplines are considered.
iii. Designing is done on several operating points and the off design characteristics are evaluated.

2.3 Cost of development

In [9] the relationship between development and cost is discussed. As mentioned earlier the industry is driven by economic consideration and the cost of achieving a performance target must be taken into consideration. The paper evaluates the tools used at Rolls Royce for the preliminary design phase of military engines and emphasizes a paradox in the preliminary design stage; there is little product knowledge but there is a powerful impact on the final design!

3 Methodology

3.1 The preliminary engine design process

The engine design process usually starts with an engine specification. The specification can either be a result of the requirements presented by a customer, or by the manufacturer itself to meet a market need.

The first step in the design process is the thermodynamic cycle analysis. The configuration of the engine, the cycle parameters and the performance of the components are selected and evaluated to meet the given specification.

When the major parameters are set by the thermodynamic analysis, the aerodynamic design of the turbomachinery and other components can begin. The number of stages, overall sizes, rotational speeds, efficiencies and other aerodynamic parameters can be determined.

Once the aerodynamic design is complete, the mechanical design of the components can begin, in this stage the mechanical properties such as stress and vibrations are evaluated.

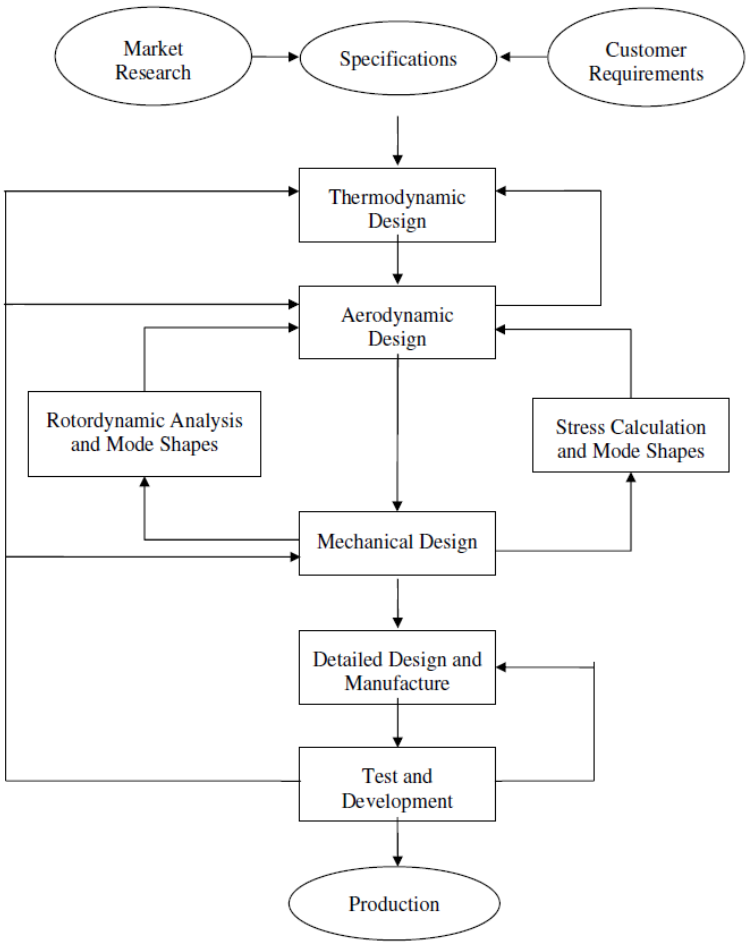

Figure 1: Preliminary engine design process [10]

This process needs constant feedback between the different disciplines, and changes in one may lead to changes in another. Figure 1 shows a schematic diagram representing a general design procedure.

This thesis will cover the thermodynamic, aerodynamic and a small part of the mechanical design. The full specification of the engine requirements can be found in the RFP [1].

3.2 Thermodynamic analysis

3.2.1 Design point and off design performance calculations

At the design point, the thermodynamic performance of the engine is evaluated at a fixed operating condition. In the case of the MJ – Haran S14 the operating condition chosen is supersonic cruise at M 1.5 at 51000ft, where the engine is expected to spend most of its time. Changing the operating condition in the design point stage would result in a different engine with a different geometry. This conditions used as a reference point.

The next step is to run *off design performance calculations*. The engine geometry is now fixed and the performance of the engine at different operating conditions is evaluated. Many off design cases may be run to ensure the engine performance over the entire operating range. Both design point and off design performance calculations are highly iterative processes [11].

3.2.2 Software description

For the thermodynamic analysis of the engine, the *Numerical Propulsion System Simulation* (NPSS) code has been used. NPSS was developed by NASA in cooperation with U.S aerospace industries with the aim to develop a state of the art simulation tool for complex systems with an open architecture for user flexibility. The code is written in C++ and allows users to add their own unique objects and calculations. The program has a built in solver with the ability to make one parameter dependent on another, and hence varying the user input of these parameters to satisfy a certain condition specified by the user [12].

3.2.3 Cycle modeling and optimization

A replica of the baseline engine was modelled as a starting point for the cycle optimization. The cycle was then modified to achieve the required thrust levels at design point. The key cycle performance data can be seen in chapter 4. All comparisons herein are to the modified baseline engine. For the initial cycle optimization, turbomachinery efficiencies and pressure losses were assumed to be the same as for the baseline engine.

3.2.3.1 Cycle efficiency

A number of different types of efficiencies can be used to characterize the performance of an aero-engine:

Propulsive efficiency – the ratio of useful propulsive energy. This is the product of thrust and flight velocity divided by the wasted kinetic energy of the jet.

Thermal efficiency – the increase of the kinetic energy of the gas stream divided by the energy of the fuel, which is the product of the fuel mass flow and the fuel LHV. For a turbofan engine, because of

the two gas streams the thermal efficiency is divided into two terms, the core efficiency and the transmission efficiency.

Core efficiency – the energy available after all the power requirements of the core stream are satisfied, which is the energy available at the core exit, divided by the energy of the fuel. This is evaluated assuming an isentropic expansion from the state at the core exit to ambient pressure.

Transfer efficiency – the quality of the energy transfer from the core stream to the bypass stream. This is the energy available at the nozzle divided by the energy at the core exit.

Overall efficiency – the ratio of useful work done in overcoming the drag of the airplane, and the energy of the fuel. For a turbofan engine, this is the product of the core efficiency, the transfer efficiency and the propulsive efficiency [13].

SFC – The mass flow of burnt fuel per unit of time per unit of output thrust [11]

Detailed formulas are provided in appendix A.

3.2.3.2 Selection of cycle parameters

The primary parameters for optimizing the cycle of a turbofan engine are the following: FPR, BPR, OPR and TIT. The definitions can be found in appendix A. These are limited by a number of mechanical design constraints such as creep, oxidation, casing rupture and vibrations. Herein the following secondary design parameters have been evaluated: Cooling air, pressure losses, turbomachinery efficiencies, power off-take, mixer efficiency and exhaust efficiency. It should be noted that the engine mass flow was kept constant in this study in order to maintain a constant engine diameter.

Fan pressure ratio

The fan pressure ratio was selected by letting NPSS solver vary the FPR to always achieve the required specific thrust. The required FPR to satisfy this condition is highly dependent on the remaining parameters in the engine, and will vary as other parameters vary. For the MJ – Haran S14, the core stream FPR and the by-pass stream FPR is assumed to be the same, which in reality may be hard to achieve due to the different blade speeds at the fan tip and the fan hub.

Bypass ratio

It can be shown that for every FPR there is an optimum BPR and vice versa. At this condition the overall energy conversion is maximized giving minimum SFC, maximum specific thrust and maximum engine overall efficiency. In [14] it is shown that for a mixed flow turbofan this occurs when the velocity ratio between the two streams $\frac{V_{BP}}{V_{core}} \sim 0{,}8$. The BPR has been selected using this relationship, letting the NPSS solver vary the BPR keeping the velocity ratio fixed at any FPR and overall condition.

η_{th}, η_{trans}, η_{ov} and SFC over the velocity ratio are illustrated in figure 2. SFN, TIT and OPR are kept constant. It can be seen that overall efficiency is at its maximum and SFC at its minimum when the velocity ratio is approximately 0,8.

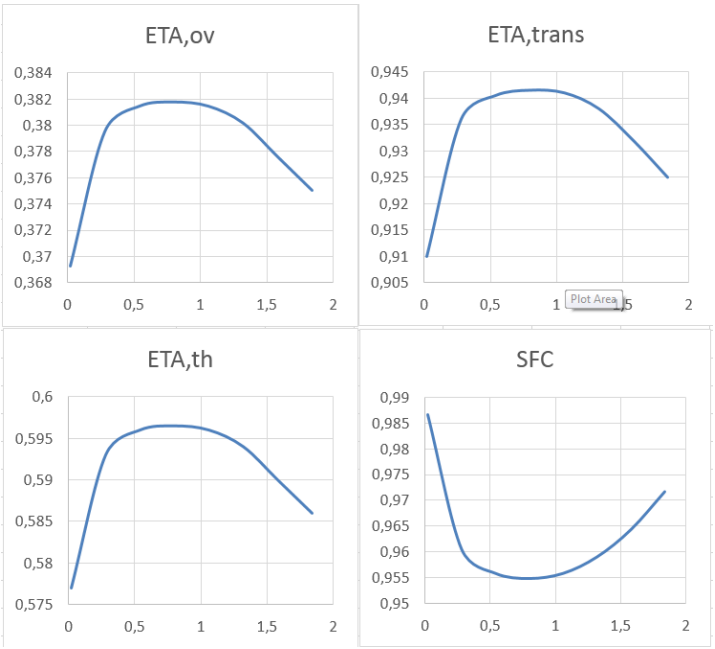

Figure 2: Different cycle efficiencies over velocity ratio in the mixer

Turbine inlet temperature

In principle, increasing the TIT and OPR will increase thermal efficiency and hence SFC. However, due to material temperature limitations, a higher TIT will need higher cooling flows for the turbines. Cooling flows essentially represent losses in the cycle and at a certain point these losses will overcome the gain in efficiency [2]. The MJ – Haran S14 uses an uncooled LPT to keep cooling flow losses to a minimum and production costs down, thus limiting the TIT.

Overall pressure ratio

For a turbofan engine, there is an optimal OPR for a given TIT where the core and thermal efficiencies are at their maximum and hence the SFC at its minimum [15]. This was found by creating diagrams of core efficiency vs OPR, using different temperatures and constant SFN, letting the NPSS solver optimize the remaining parameters. A generic diagram showing this relationship for different types of cycles at a specific TIT can be seen in figure 3.

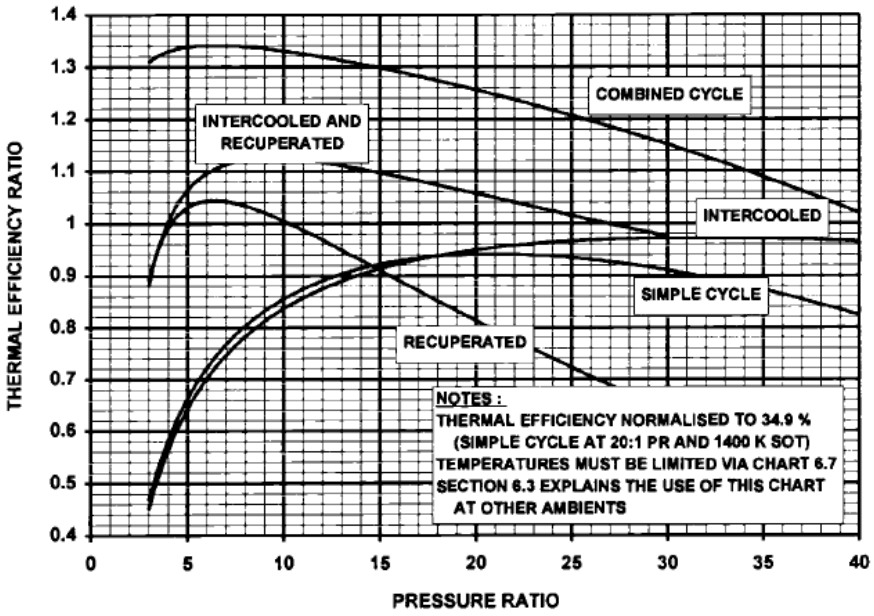

Figure 3: η_{th} over OPR for different types of cycles [11]

Cooling flows

The necessary cooling flows have been calculated using the method described in [16]. The required cooling flow will depend on the cooling flow efficiency, which varies depending on the technology being used. The calculations roughly correspond to a film/cross flow impingement technology. Two cooling flows have been considered for the HPT: one for the NGV and one for the rotor. An upper limit of 18% of the HPC inlet flow was decided to avoid excessive losses. The cooling flows were added as a variable to the NPSS solver to keep constant blade metal temperatures based on the blade temperatures for modern designs under all overall conditions. The flow is taken from the last stage of the HPC to assure sufficient pressure.

Power off-take

The power off-take from the HPT has been set to 100hp in accordance to the RFP [1].

3.3 Aerodynamic design

The aerodynamic design can commence when the flow properties are defined from the thermodynamic analysis. In this process, the dimensions, pressure losses, efficiencies, and other aerodynamic parameters for the different components can be determined and evaluated.

3.3.1 Software description

MATLAB is a widely used numerical computing environment and programming language suitable for a range of applications. Its ability to read data from external sources, built in functions, advanced plotting functions and extensive documentation made it an appropriate choice for this project [17].

3.3.2 Turbomachinery

The initial turbomachinery sizing requires a few assumptions from the designer in order to proceed with further analysis of the component. Based on these assumptions together with the fluid properties from the thermodynamic analysis the areas, rotational speeds, blade speeds, number of stages, stage loading etc. can be determined. The initial sizing procedure can be found in [18], where guidelines for initial assumptions of the necessary parameters are also given. With the initial sizing procedure done, the parameters described in the following sections can be evaluated, and the turbomachinery properties can be modified to assure adequate performance.

3.3.2.1 Velocity triangles

In order to design the blades, the power input per stage needs to be related to velocity triangles. These give an indication of how the blades change from the hub to the tip by showing the variations in velocity.

The velocity triangles for a typical stage at the mean radius can be seen in figure 4. The fluid approaches the rotor with an absolute velocity of C_1 at an angle α_1 relative to the axial direction. By combining C_1 vectorially with the blade speed U, the velocity relative to the blade V_1 at an angle β_1 relative to the axial direction can be found. As the flow passes through the rotor, the absolute velocity of the fluid increases leaving the rotor with a velocity V_2 at an angle β_2. With the axial velocity C_{a1} constant over the stage, V_2 can be found and the outlet velocity triangle constructed by combining V_2 and U vectorially to give C_2 at the angle α_2. The fluid then passes to the stator where it's diffused to a velocity C_3 at an angle α_3. Generally α_3 approximately equals α_1 and C_3 approximately equals C_1 so that the fluid is prepared for entry into another similar stage [19].

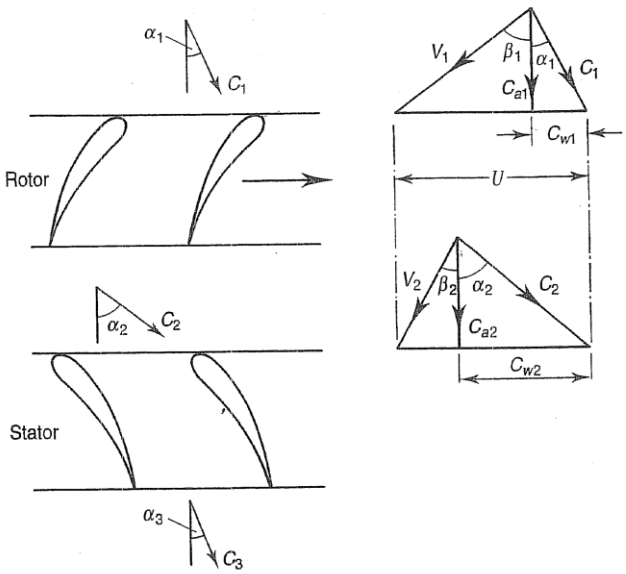

Figure 4: Velocity triangles for a typical compressor stage [19]

In this work the axial velocity has been determined assuming values of $M_{ax,in}$ and $M_{ax,out}$ based on guidelines given in [18] with a linear interpolation within the component. The velocity triangles have been calculated at the hub, mean, and tip of each blade of the turbomachinery components. With regard to radial equilibrium, the exponential blading method was used to determine the angles and the velocities at the hub and the tip. The necessary equations and formulas can be found in [19].

A number of aerodynamic properties have been evaluated to achieve an adequate turbomachinery performance including: degree of reaction, diffusion factor, De Haller number, stage loading, flow coefficient and deflection. Detailed formulas are provided in appendix A.

Degree of reaction

The degree of reaction is defined as the ratio between the static enthalpy change in the rotor and that of the whole stage. It provides a measure to the extent of which the rotor contributes to the overall pressure difference in the stage [19]. For a compressor, this should typically be in the range of 0,5 – 0,8 [20], while for a turbine 0,3 – 0,5 [11].

Diffusion factor

The air passing over an airfoil will accelerate on the convex side, leading to a drop in static pressure. On the concave side, the air will decelerate. The losses in a blade row arise primarily from growth of boundary layers on the two blade sides. At the blade trailing edge the boundary layers come together forming a wake, causing a local drop in total pressure. Thick boundary layers, causing high losses have been found in regions where rapid velocity changes occur. The diffusion factor concept was developed by NACA based on cascade testing. For the rotor hub region and stators the losses are unaffected up to a diffusion factor of 0,6. In the rotor tip region, the losses grow rapidly at a diffusion factor above 0,4 [19].

De Haller number

The de Haller number is defined as the velocity ratio of the trailing edge and the leading edge of a blade or a vane. This is a simple measurement of diffusion used in preliminary design work. The De Haller number should exceed 0.72. For final calculations, the diffusion factor is preferred [19].

Stage loading

Stage loading is a measure of how much work is demanded by a turbomachinery stage and therefore the required "turning" of the flow. It is defined as the enthalpy change per unit mass flow of air divided by the blade speed squared. A lower stage loading leads to a higher efficiency, but in turn, more stages are required [11].

Flow coefficient

The flow coefficient relates primarily to component size, and if it is non-optimal to the efficiency. It is defined as the axial velocity divided by the blade speed. A typical value is 0,4 – 0,8 [20].

Deflection

The deflection is the difference between the angle of the relative velocity of the leading edge and the trailing edge. It is a direct measure of flow turning. A high deflection would imply a high rate of diffusion in a compressor or acceleration in a turbine.

3.3.2.2 Flow path

The flow paths for the turbomachinery components have been evaluated using three different design approaches: constant mean diameter, constant outer diameter and constant inner diameter. The flow path selection will influence some of the above mentioned parameters, and they all have some advantages and disadvantages [19]. In modern designs an intermediate choice of constant inner and constant outer is often made. Figure 5 shows the three designs of a compressor.

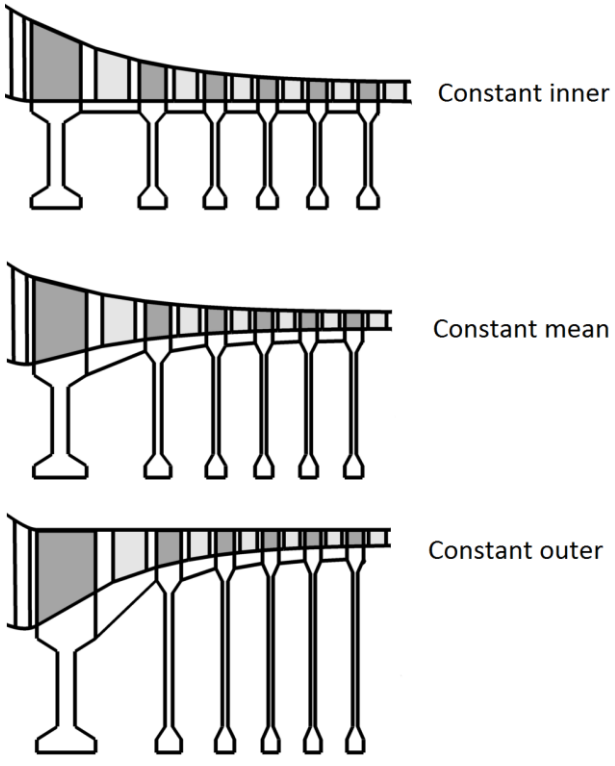

Figure 5: Different types of flow paths

3.3.2.3 Turbomachinery efficiencies

In an ideal compression or expansion process the assumption is made that there is no change in entropy. In a real process however, several losses take place as the fluid flows through the component resulting in an entropy generation. For a compressor this results in a higher temperature and enthalpy, and hence work, at a given pressure ratio compared to what would be expected from an ideal process. For a turbine, the outlet pressure will always be lower at a given power output requirement [15]. The two most common ways to account for losses in the turbomachinery components is the isentropic and polytropic efficiency.

Isentropic efficiency

The isentropic efficiency of a compressor is defined as the ratio between the change in enthalpy for an ideal process, and the change in enthalpy for the actual process. For a turbine the isentropic efficiency is defined as ratio between the change in enthalpy for the actual process, and the change in enthalpy for the ideal process [15].

Polytropic efficiency

The isentropic efficiency can be misleading when comparing compressors and turbines with different pressure ratios or at different inlet conditions. If the necessary calculations are performed for each stage of a multistage component, with the assumption that each stage operates at the same isentropic efficiency, the result would be that the efficiency of the whole component is lower than the stage efficiency. Consequently isentropic efficiency is not a suitable parameter when performing optimization studies. For such studies, the polytropic efficiency can be used. The polytropic efficiency can be defined as the isentropic efficiency at an infinitely small stage in the compression or expansion process, such that it can be assumed constant throughout the entire process [15]. Therefore the turbomachinery polytropic efficiencies have been used in this project.

The efficiency calculations are based on outputs from both the thermodynamic analysis and the sizing procedure, and are based on the following parameters: Entry into service correction, Reynolds number index effect, size variation and normalized efficiency. These are all based on empirical data. The method used can be found in [21].

3.3.3 Combustion chamber

In order to commence the combustion chamber sizing, a few assumptions need to be made by the designer. These assumptions are based on the guidelines in [22] where the full sizing procedure can also be found. A typical burner can be seen in figure 6.

Loading

Combustor volume must be derived considering the combustor loading at a number of flight conditions. At static sea level maximum power the combustor loading should be less than $10\,\frac{kg}{s\cdot atm^{1.8}\cdot m^3}$. A critical point for the burner is the ability to relight during windmilling following an engine flameout. In order to achieve this the designer must make sure that the combustor loading at the highest required altitude and lowest flight Mach number for relight does not exceed $300\,\frac{kg}{s\cdot atm^{1.8}\cdot m^3}$ [23]. To minimize the volume of the burner, the loading should be close to 300 at windmilling conditions. A smaller burner however, leads to a higher pressure loss. The definition can be found in appendix A.

Residence time

The residence time depends on the length of the liner and the Mach number after the diffuser, and should typically exceed 3ms. Long residence times however, can result in increased NOx.

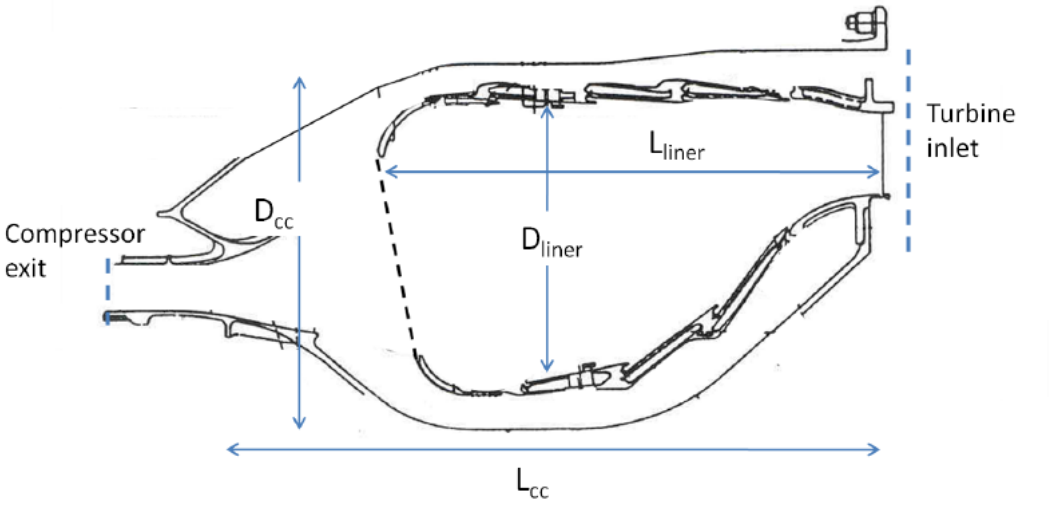

Figure 6: Typical burner [22]

Pressure loss

A pressure loss occurs in the combustion chamber due to skin friction and the rise in temperature. The skin friction loss is called the cold loss and accounts for approximately 90% of the total pressure loss. The loss due to rise in temperature is called the fundamental loss and accounts for the remaining 10% [23]. The pressure loss has been estimated using the method described in reference [22] and is dependent on the maximum area of the burner, the PLF and the inlet T_0 and P_0. The PLF is an assumed value and is typically in the range of 20 to 25 [23].

Efficiency

The efficiency of the burner can be found from a chemical analysis of the combustion products. Knowing the fuel to air ratio and the proportion of incompletely burnt constituents, it is possible to calculate the ratio of the actual energy released to the theoretical quantity available. Due to a number of reasons this is a very complicated approach. In practice, the combustion is complete at high-power to mid-power conditions [19] and the burner efficiency has therefore been assumed to be 0,9999.

3.3.4 Internal ducts

The ducts have been designed using cubic splines to allow for smooth surfaces between the components trying to minimize the pressure loss. However, no pressure loss calculations have been performed, the losses are assumptions based on the guidelines given in reference [11].

3.3.5 Inlet

Due to time limitations, only a basic 2D/axisymmetric inlet using oblique shocks to diffuse the incoming air has been designed. Tabulated values of normal shock properties found in reference [24] have been used to calculate the total pressure loss and new Mach numbers after the shocks. The inlet has been designed to create an oblique shock at the inlet start, reducing the Mach number to a value close to one, after which a normal shock at the venturi reduces the value to below one. After this, the velocity is diffused in the divergent part using the continuity equation to an acceptable value before entering the fan. These calculations assume an isentropic flow. To compensate for this the total pressure loss has been multiplied by a factor of 0,997 for the subsonic region to account for pressure losses due to skin friction. The necessary formulas and equations can be found in [24]. With

the angles and areas known, the geometry of the inlet has been calculated using standard trigonometric relations.

3.3.6 Nozzle

A convergent – divergent nozzle lets the flow expand to ambient pressure, which for an isentropic process produces maximum thrust [11]. However, due to skin friction losses and the extra weight and length, a con - di nozzle is only a viable option if the nozzle pressure ratio is greater than about three [15] which tends to be the case for supersonic engines due to the high ram pressure ratio. The thrust loss associated with flow angularity increases sharply at great exhaust angles, therefore the angle of the divergent section should be less than 30 degrees [11].

To account for losses in the nozzle, different coefficients are used, the definitions of these may vary between different manufacturers. In this thesis the thrust coefficient, CV and the angularity coefficient C_θ are used. CV is defined accordingly to [15]. This coefficient gives the actual thrust from the thrust that could be achieved by an ideal con – di nozzle by accounting for friction and flow non-uniformity. The value of CV has been assumed based on guidelines given in [11]. C_θ is defined as $0,5 \cdot (1 + \cos(\alpha))$, where α is the half angle of the divergent section [25]. The area of the nozzle inlet, throat and exit is calculated in the thermodynamic analysis.

3.3.7 Mixer

The use of a mixer to combine the hot and cold stream prior to the exhaust has a few advantages compared to using two separate exhausts: a small gain in net thrust and SFC can be achieved, the optimum fan pressure ratio at a constant specific thrust is lower leading to a lower weight and cost for both the fan and the LPT, the jet noise is lower due to the velocity of the mixed stream being significantly lower than the core stream of a separate jets engine. In the decision whether to adopt a mixer these advantages need to be balanced against the disadvantages of the extra weight and cost [11]. For the thrust gain to be maximized the mixing needs to be complete (i.e. a mixer efficiency of 100%), this would require a large and heavy mixer, which in turn would require more thrust [1]. Therefore a compromise between mixer efficiency and thrust gain is necessary. Figure 7 shows the theoretical gross thrust gain by introducing a mixer assuming that: the FPR is at its optimum, the mixing efficiency is at 100% and no pressure loss is accounted for.

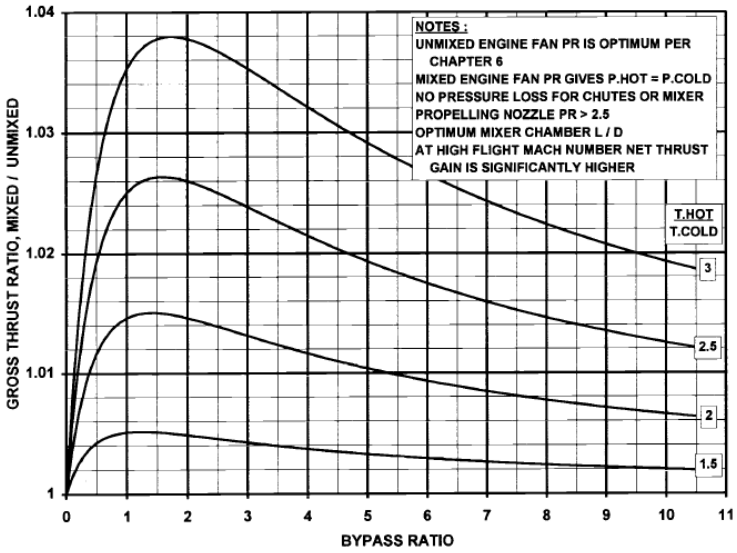

Figure 7: Theoretical thrust gain due to mixing [11]

An approximate length and mixer efficiency have been estimated based on guidelines in [11]. To perform mixer calculations the designer must set the Mach number of the primary incoming stream, after which the Mach number of the second stream is varied until the static pressures of the two streams are equal in the mixer. The Mach number has been set based on guidelines given in [19]. The mixer area for the two streams is calculated in the thermodynamic analysis.

3.3.8 Iterations

The efficiencies of the components highly depend on the choices made in the aerodynamic design, once these are set, the new values need to be inputs to the thermodynamic analysis, which in turn will generate new optimum values for the key parameters, and the aerodynamic design will need to be evaluated again. As mentioned earlier constant feedback is required between the different disciplines. Iterations were performed until the residual of the turbomachinery efficiencies were less than 0,0005.

3.4 Mechanical design

3.4.1 Software description

The discs have been designed using T – AXI DISK V2.5, a software developed primarily for education purposes. The system can be used to design multistage compressors and turbines from a small number of physical design parameters [26]

3.4.2 Discs

To carry out the disc analysis, the designer needs the aerodynamic properties of the component, such as stage geometry, RPM and temperatures. Due to time limitation, the disc analysis has only been carried out on the HPC and the HPT where the disc stresses are the highest due to high disc speeds. The RPM of the HP shaft is often limited by disc stresses in the HPT rather than the first stage $M_{tip,rel}$ for the HPC [27]. The disc designs: hyperbolic, web, continuous slope and ring can be seen in figure 8.

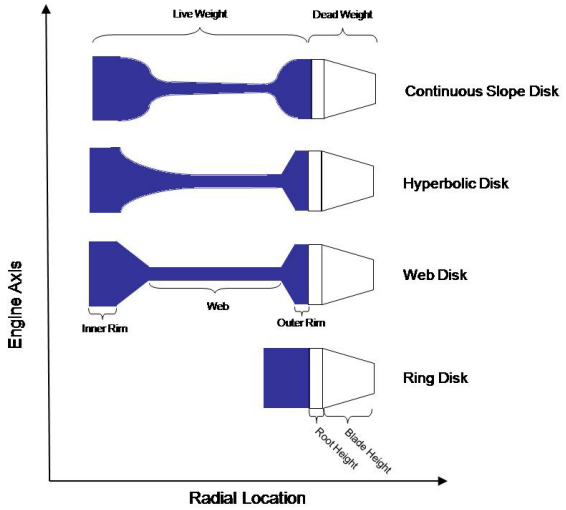

Figure 8: Different types of disc designs [28]

Target safety line

The target safety line is a safe margin until the material starts to yield, this has been kept at the default 10%.

Optimization

The optimization was carried out with the T – AXI DISK built in function, parametric disc, which optimizes the disc in order to get a design that meets the target safety line and has the lowest possible weight. Parameters such as rim width, bore width, bore radius etc. need to be set by the designer before the optimization can start.

3.4.3 Shafts

The mechanical efficiencies of the shafts are input parameters to the thermodynamic cycle analysis, in this work they are assumed to be 99,5% for both shafts [11]. No further shaft assumptions or calculations have been made.

4 Results and discussion

4.1 Baseline engine

The modified baseline engine performance data, which served as a starting point for the cycle optimization can be seen in table 1. A schematic 2D view of the engine can be seen in figure 9.

Altitude	$15545m$	***HPT rotor cooling***	5%
Mach	1,5	***LPT NGV Cooling***	2,5%
Gross Thrust	$82270N$	***LPT rotor cooling***	0,5%
Net Thrust	$42500N$	$\eta_{poly,fan}$	0,8914
Mass flow	$90kg/s$	$\eta_{poly,HPC}$	0,9180
SFN	$472Ns/kg$	$\eta_{poly,HPT}$	0,9136
SFC	$1{,}068lbm/(hr \cdot lbf)$	$\eta_{poly,LPT}$	0,9151
OPR	16	η_{core}	0,579
TIT	$1472K$	η_{prop}	0,625
BPR	0,3	η_{tran}	0,943
FPR	3,29	η_{th}	0,546
HPT NGV Cooling	6%	η_{ov}	0,341

Table 1: Key data for the baseline engine

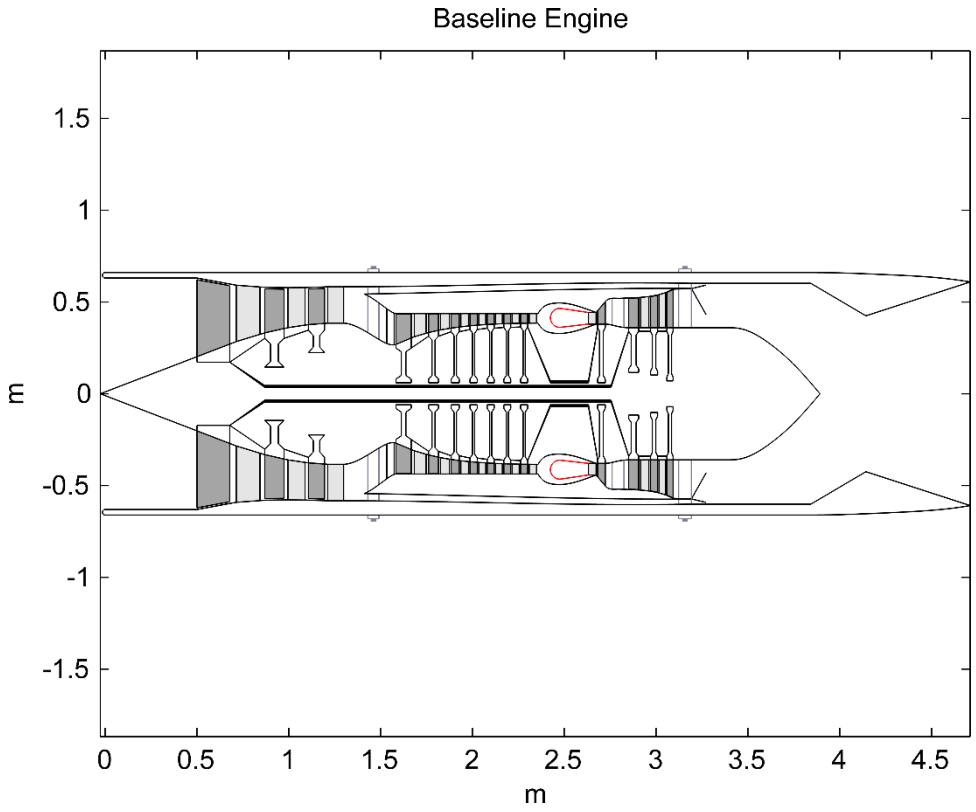

Figure 9: Section view baseline engine

4.2 Cycle optimization

A two spool axial flow low by-pass turbofan configuration was selected for the MJ – Haran S14. The engine layout with flow stations can be seen in figure 10.

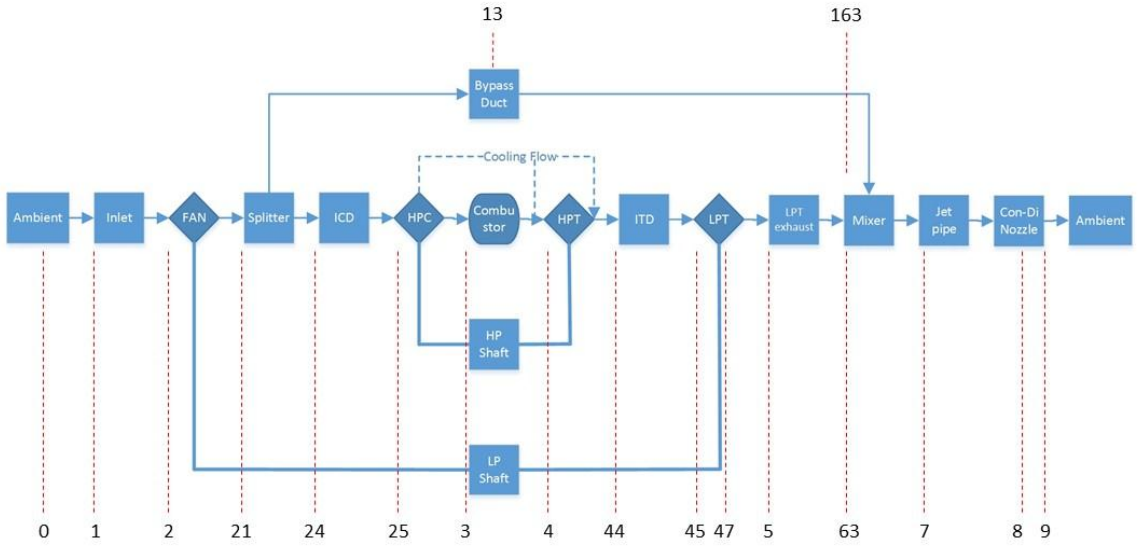

Figure 10: Engine layout with flow stations

4.2.1 TIT and OPR optimization

The optimum OPR for different TIT:s can be seen in figure 11. SFN and polytropic efficiencies have been kept constant. Other parameters have been varied to keep the optimum interrelationships between the components. Figure 11 shows that increasing TIT and OPR increases the core efficiency. The design is however limited by the blade metal temperature in the turbines. At cruise condition this temperature was set to 1150K which is representative of a single crystal metal with thermal barrier coating in the HPT and Inconel 718 in the LPT. Table 2 shows the required cooling flow to keep this temperature in the HPT, and the inlet temperature of the uncooled LPT for each of the TIT:s at its optimum OPR.

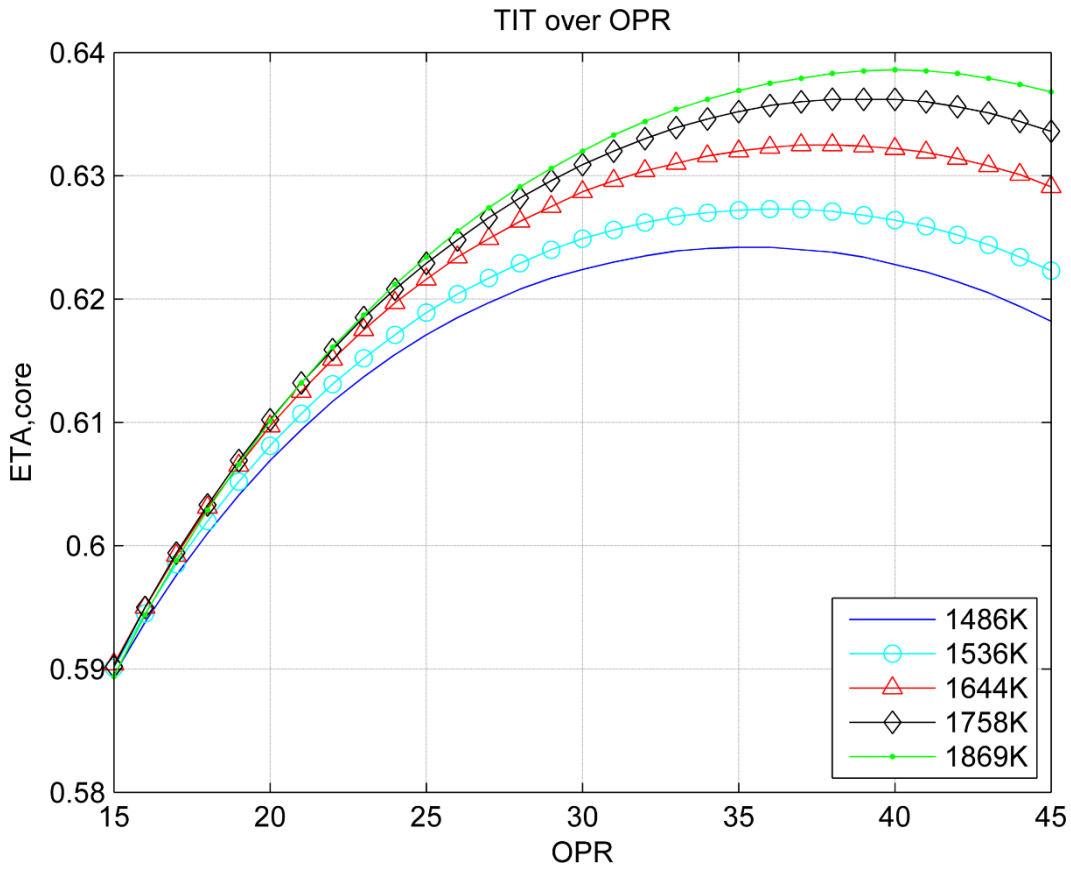

Figure 11: Optimum OPR at different TIT: s.

TIT (K)	Opt. OPR	Required HPT cooling flow (%)	LPT inlet temperature (K)
1486	35	9.8	1052
1536	37	12	1082
1644	38	16.2	1150
1758	40	20.2	1218
1869	41	24	1278

Table 2: Required HPT cooling flow and LPT inlet temperature

Table 2 shows that the maximum TIT in order to keep the desired LPT inlet temperature is 1644K, at this temperature the cooling flow for the HPT is also within acceptable limits. Based on this, the TIT has been set to 1644K and the OPR to 38.

Figure 12 shows the relationship between core efficiency, thermal efficiency, overall efficiency and SFC at the chosen TIT. It can be seen that the maximum values occur at approximately the same OPR, which also corresponds to the lowest value of SFC. The propulsive and transfer efficiencies are relatively constant over this range, and are excluded in the diagram.

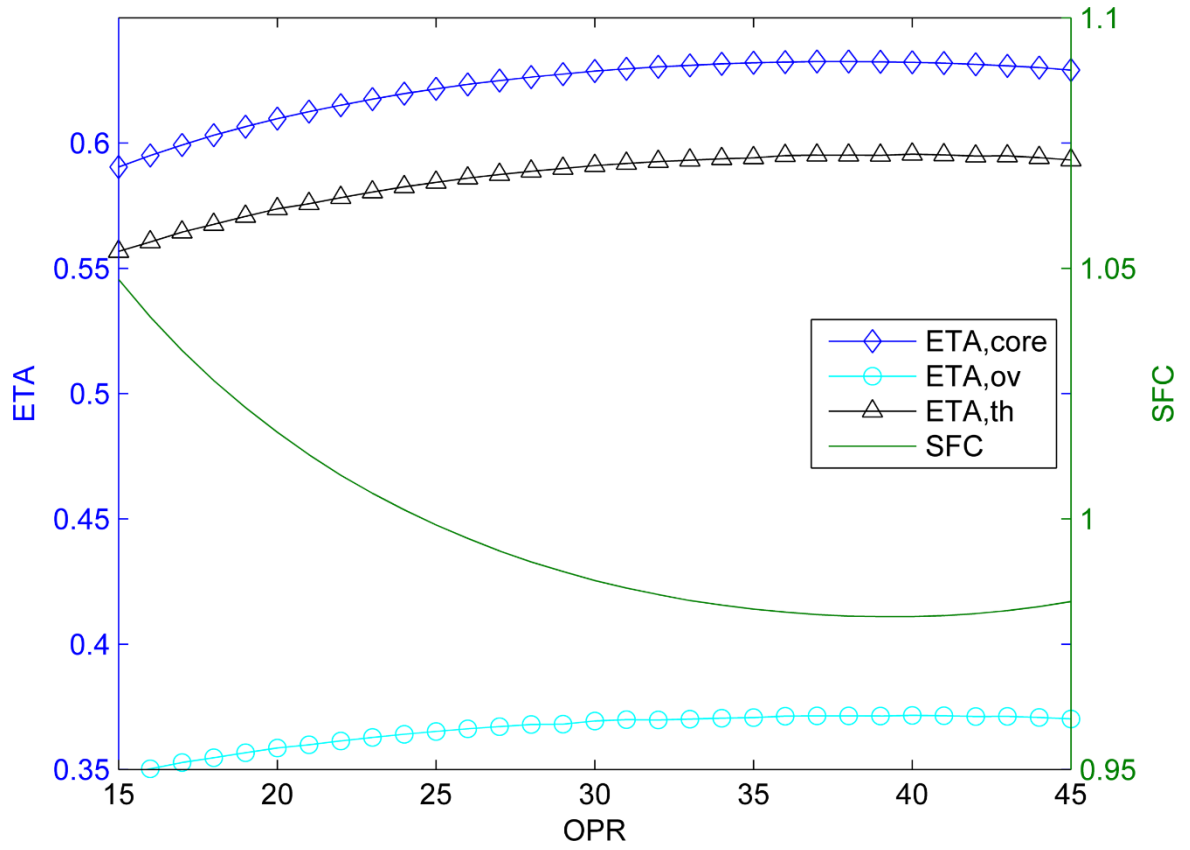

Figure 12: Efficiencies over OPR

With the OPR and TIT set, the remaining parameters were found using the interrelationships described in chapter 3. The key parameters for the engine design point cycle can be seen in table 3. A full output of the engine cycle performance data can be found in appendix B.

Altitude	$15545m$	***HPT NGV cooling***	9,7%
Mach	1,5	***HPT rotor cooling***	6,5%
Gross Thrust	$82270N$	$\eta_{poly,fan}$	0,901
Net Thrust	$42500N$	$\eta_{poly,HPC}$	0,941
Mass flow	$90kg/s$	$\eta_{poly,HPT}$	0,91
SFN	$472Ns/kg$	$\eta_{poly,LPT}$	0,934
SFC	$0{,}98lbm/(hr \cdot lbf)$	η_{core}	0,632
OPR	38	η_{prop}	0,624
TIT	$1644K$	η_{tran}	0,941
BPR	0,4	η_{th}	0,595
FPR	3,93	η_{ov}	0,371

Table 3: Key parameters for design point cycle

A schematic 2D view of the complete engine can be seen in figure 13. The engine with inlet can be seen in figure 14. Note that the discs are preliminary, the final HPC and HPT discs can be found in appendix D.

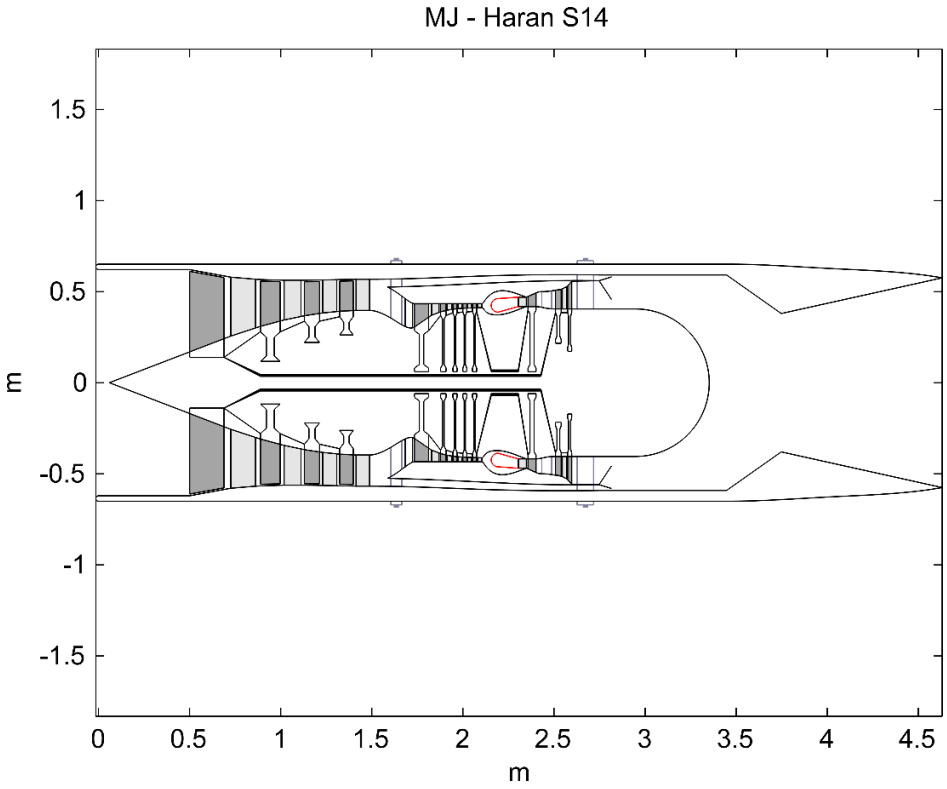

Figure 13: The MJ – Haran S14 section view

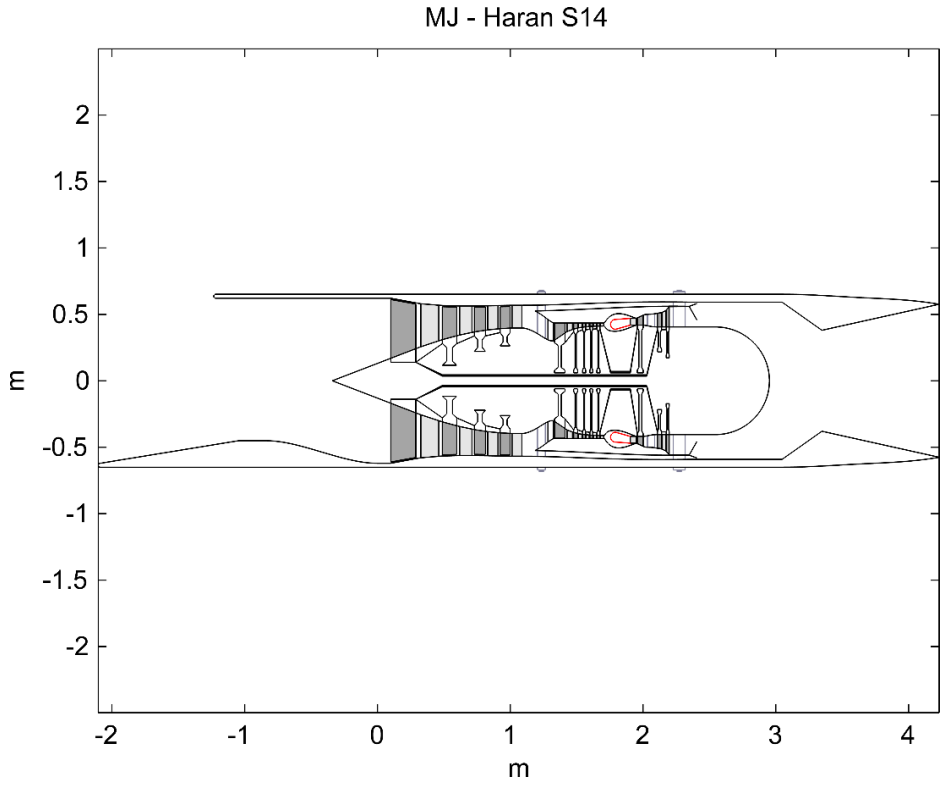

Figure 14: The MJ – Haran S14 section view with supersonic inlet

4.3 Component design

4.3.1 Inlet

A 2D view of the inlet, with the shocks represented as dotted lines can be seen in figure 15. The inlet has a total pressure recovery of 0,983 and a total length 2,088 m. The deflection angle θ was set to 9,26° to achieve maximum pressure recovery in combination with the following normal shock at design point. The corresponding β angle is 55°. The remaining inlet data can be seen in table 4.

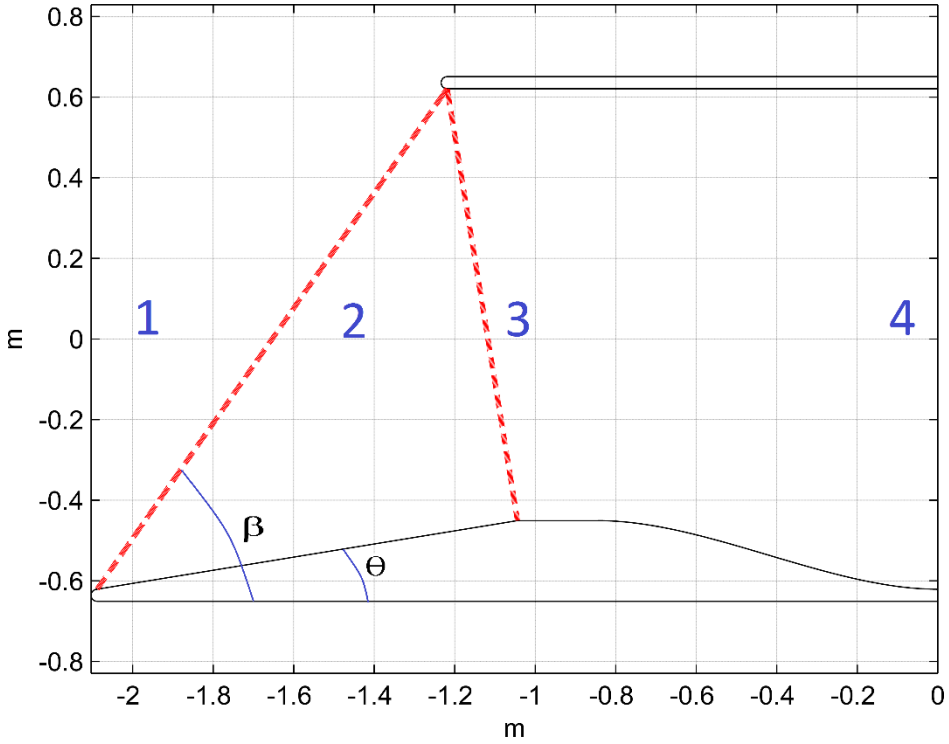

Figure 15: Supersonic inlet with flow stations

Station	Mach number	PR	Area(m^2)
1	1,500	–	–
2	1,152	0,9897	–
3	0,874	0,9966	0,992
4	0,650	0,9970	1,211

Table 4: Inlet data

4.3.2 Internal ducts

The assumed pressure ratios and the lengths of the internal ducts can be seen in table 5 and a schematic view can be seen in figure 16.

Duct	Bypass	Intercompressor duct	Interturbine duct	LPT exhaust	Jet pipe
PR	0,97	0,98	0,98	0,985	0,99
Length	1,163m	0,149m	0,107m	0,150	0,5

Table 5: Duct data

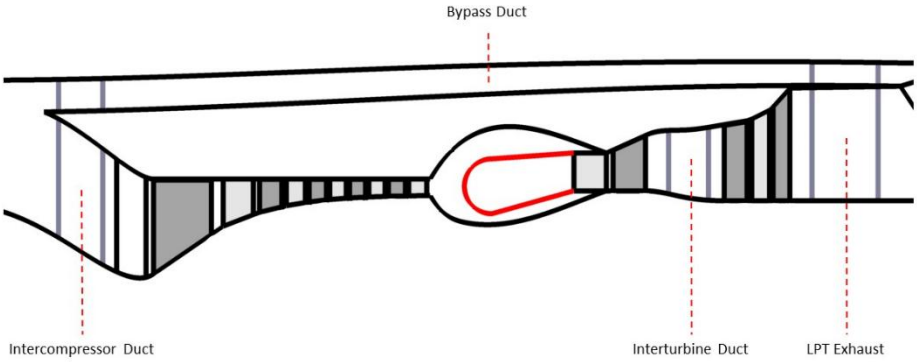

Figure 16: Ducts

4.3.3 Compressors

In order to use an uncooled LPT, a two shaft no-booster design was chosen to maximize the work done by the HPT, thus lowering the inlet temperature to the LPT. The tip clearance has been set to 1% of the blade height. The blade spacing has been set to 20% of the upstream chord [11]. The two compressors can be seen on a Smith chart [29], based on the average stage load and flow coefficient in figure 17.

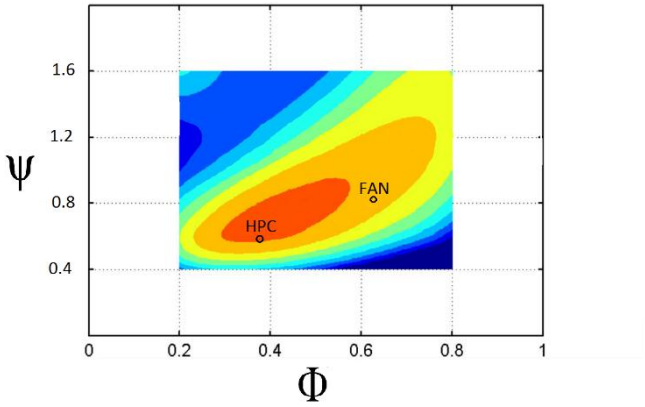

Figure 17: Stage load over flow coefficient for the FAN and HPC

4.3.3.1 Fan

With a FPR of 3,93, a four stage fan was deemed necessary to achieve satisfactory performance. The fan flow path is a result of a linear interpolation starting from the hade angle, gradually decreasing to

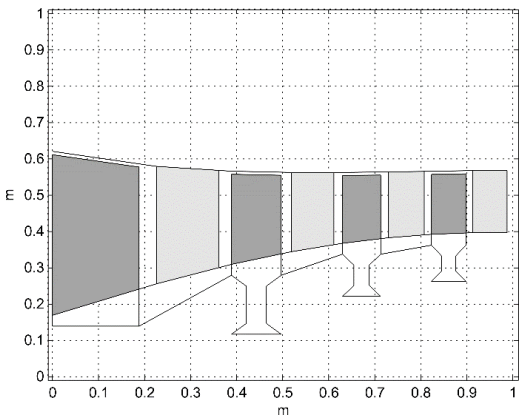

Figure 18: Fan component

zero at the last stage stator outlet. The hade angle was selected to 21° in order to achieve a decent blade velocity at the first stage rotor hub exit. $M_{ax,in}$ has been set high to keep the area to a minimum.The low pressure shaft RPM was set to reach a $M_{tip,rel}$ close to 1,45. The fan can be seen in figure 18.

Table 6 shows some key fan data. Figure 19 shows the fan velocity triangles at the mean blade and table 7 shows the velocity triangles data at the mean blade. A full output of stage by stage performance can be found in appendix C. It can be seen in the appendix that the first stage hub velocity triangles are unrealistic. This is the result of a high stage loading at the hub due to a big enthalpy change and a low blade speed which indicates that the fan pressure ratio has to vary from a lower value at the hub region to a higher value at the tip.

$M_{ax,in}$	0,65	$Number\ of\ stages$	4
$M_{ax,out}$	0,38	$Avg.\psi$	0,82
AR_{in}	2,40	$Avg.\phi$	0,63
AR_{out}	2,30	$Avg.Temp\ rise_{stage}$	$42{,}3K$
$Hub/Tip-ratio_{in}$	0,27	η_{poly}	0,901
$Hub/Tip-ratio_{out}$	0,69	$M_{tip,rel,in}$	1,43
EIS	2025	RPM/U_{tip}	7000/455,15
$s/c-ratio$	1,20	$Total\ length$	$0{,}9876m$
$Hade\ angle_{in}$	21°	$Max\ diameter$	$1{,}2418m$

Table 6: Key fan data

$Stage$	1	2	3	4
β_1	53	52	56	58
β_2	34	27	34	39
α_1	0	12	13	22
α_2	34	45	47	50
C_{a1}	222	212	197	177
C_{a2}	222	212	197	177
U_1	290	321	340	351
U_2	303	331	346	353
V_1	365	348	356	331
V_2	269	239	238	226
C_1	222	217	202	190
C_2	269	300	286	274
ϕ	0,77	0,66	0,58	0,50
ψ	0,94	0,89	0,79	0,65
$Deflection$	18	25	22	19
$Reaction$	0,74	0,60	0,63	0,60
$Diffusion$	0,34	0,46	0,47	0,47
$deHaller$	0,74	0,69	0,67	0,68
$Temp.rise$	39	45	45	39

Table 7: Fan velocity triangles data at mean blade

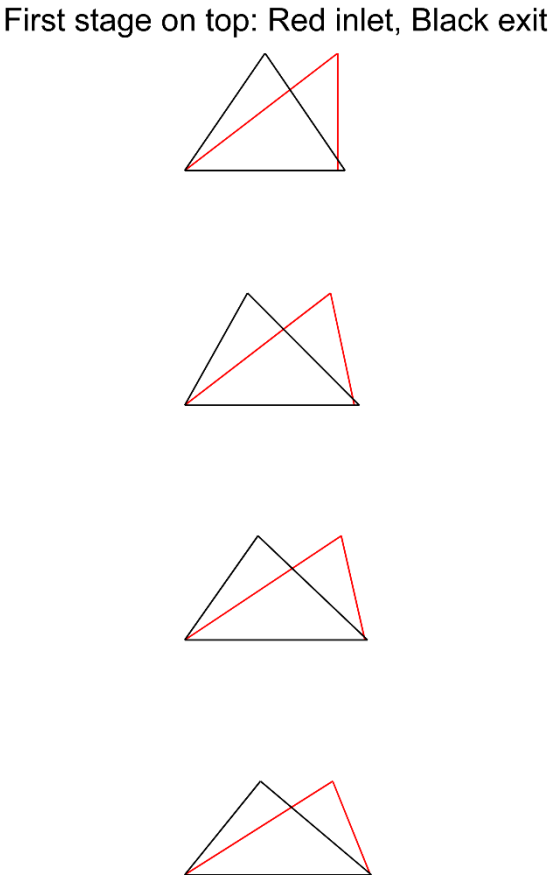

Figure 19: Velocity triangles for the fan at mean blade

4.3.3.2 HPC

A five stage constant outer diameter design was chosen for the MJ – Haran S14. This configuration allows for high hub and mean blade speeds through all stages, which reduces the stage loading. The first stage hub to tip ratio was chosen for an optimal radius of the compressor. Placing it lower would lead to higher pressure losses in the duct following the splitter due to the steep angle, placing it higher would lead to a lower RPM in order to keep $M_{tip,rel}$ at reasonable values, which in turn could lead to more stages. The final radius is a compromise between these conflicting requirements. To keep the diffusion factor at the tip below 0,4, the reaction has been adjusted to reduce from 0,75 at the first stage towards 0,5 at the last stage. With a 50% reaction the blades are symmetrical $\alpha_1 = \beta_2 = \alpha_3, \beta_1 = \alpha_2$ giving the most efficient diffusion over the stage [19]. However, a 50% reaction was not achievable with five stages. An IGV was implemented to increase the absolute velocity of the first stage, allowing a higher rotational speed while maintaining the same $M_{tip,rel}$. The HPC component is illustrated in figure 20. Note that the discs are preliminary, the final disc design can be seen in appendix D.

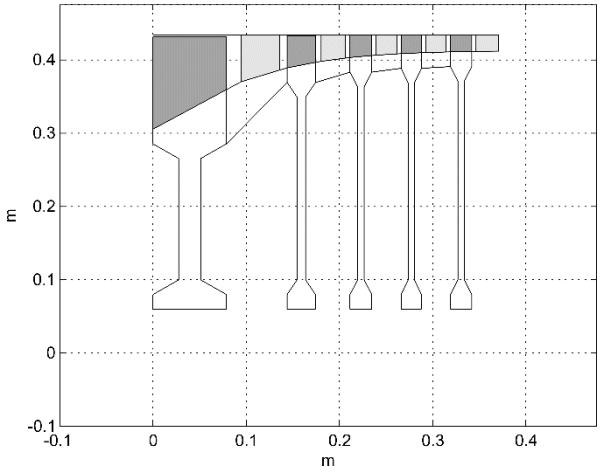

Figure 20: HPC component

Table 8 shows some key compressor data. Figure 21 shows the velocity triangles at the mean blade and table 9 shows the velocity triangles data at mean blade. A full output of stage by stage performance for the HPC can be found in appendix C.

$\boldsymbol{Number\ of\ Stages}$	5	$\boldsymbol{M_{ax,in}}$	0,52
$\boldsymbol{Avg.\psi}$	0,58	$\boldsymbol{M_{ax,out}}$	0,33
$\boldsymbol{Avg.}\phi$	0,38	$\boldsymbol{AR_{in}}$	1,63
$\boldsymbol{Avg.Temp\ rise}$	$89{,}8K$	$\boldsymbol{AR_{out}}$	0,93
$\boldsymbol{\eta_{poly}}$	0,941	$\boldsymbol{Hub/Tip-ratio_{in}}$	0,70
$\boldsymbol{M_{tip,rel,in}}$	1,34	$\boldsymbol{EIS}$	2025
$\boldsymbol{RPM/U_{tip}}$	13500/613,8	$\boldsymbol{s/c\ -ratio}$	1,2
$\boldsymbol{IGV\ angle}$	18°	$\boldsymbol{Total\ length}$	$0{,}37m$

Table 8: Key HPC data

Stage	**1**	**2**	**3**	**4**	**5**
$\boldsymbol{\beta_1}$	67	67	65	67	68
$\boldsymbol{\beta_2}$	52	57	54	57	58
$\boldsymbol{\alpha_1}$	18	15	26	20	24
$\boldsymbol{\alpha_2}$	48	46	52	51	52
$\boldsymbol{C_{a1}}$	221	225	223	216	205
$\boldsymbol{C_{a2}}$	221	225	223	216	205
$\boldsymbol{U_1}$	523	582	592	596	597
$\boldsymbol{U_2}$	561	587	594	597	598
$\boldsymbol{V_1}$	568	568	534	560	546
$\boldsymbol{V_2}$	357	417	380	394	389
$\boldsymbol{C_1}$	233	233	247	230	225
$\boldsymbol{C_2}$	328	322	361	343	337
ϕ	0,42	0,39	0,38	0,36	0,34
$\boldsymbol{\psi}$	0,66	0,57	0,56	0,57	0,54
Deflection	15	9	11	11	10
Reaction	0,70	0,75	0,67	0,71	0,70
Diffusion	0,47	0,36	0,42	0,42	0,41
deHaller	0,63	0,73	0,71	0,70	0,71
Temp.rise	87	92	92	92	87

Table 9: HPC velocity triangles data at mean blade

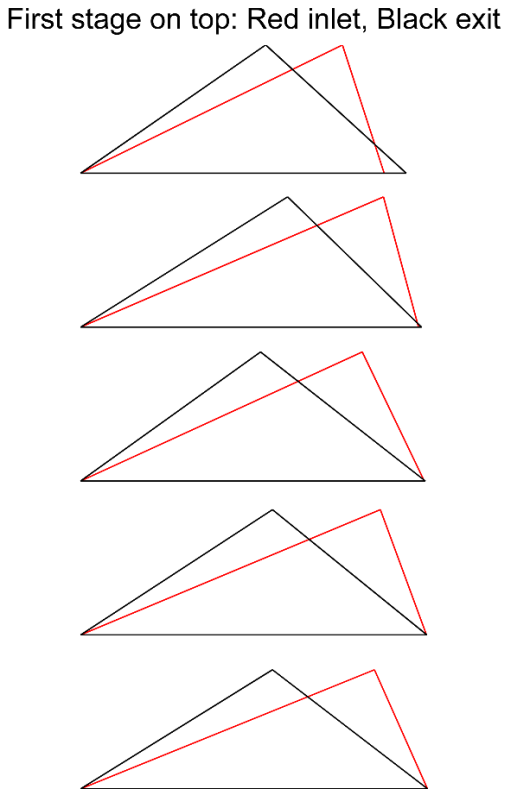

Figure 21: Velocity triangles for the HPC at mean blade

4.3.4 Combustion chamber

An annular combustor was chosen for the MJ – Haran S14 due to its compactness and clean aerodynamic design. The combustor has been sized to maintain a reasonable pressure loss, while allowing for relight at windmilling conditions. M_{ax} was set to allow for a residence time in excess of 3ms. A slope angle of 8° was chosen in order to increase the HPT radius, improving its stage loading. The combustor is shown in figure 22 and data for the combustor can be seen in table 10.

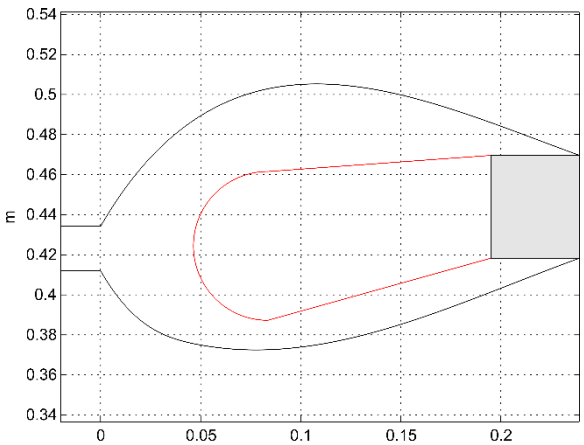

Figure 22: Combustor component

dP/P_{in}	4,11	M_{ax}	0,04
Residence time	$4ms$	**PLF**	23
Loading at Cruise	1,15	L_{liner}/D_{liner}	2
Loading at Windmilling	231	L_{cc}/D_{cc}	1,75
Pattern Factor	0,35	V_{cc}/V_{liner}	0,5
V_{cc}	$0{,}059m^3$	**Efficiency**	0,999
V_{liner}	$0{,}029m^3$	**Stochiometric Temp.**	$2300K$
Slope angle	8°	**Total length**	$0{,}195m$

Table 10: Key combustor data

4.3.5 Turbines

A constant hub design was chosen for the turbines. This configuration allows for a higher blade speed due to the increasing blade tip radius, which reduces the stage loading. The loss coefficient λ_N was set to 0,05, at this value the stator blades are convergent, which allows for good performance over a variety of power conditions [19]. To avoid choking the turbines, the angle $\alpha_{3,mean}$ has been adjusted to satisfy the condition $\left(\frac{P_{01}}{P_2}\right) < P_{critical}$. The highest relative Mach number occurs at the inlet hub. This value needs to be kept below 0,75 [19] to avoid high pressure losses due to shock waves. The tip clearance has been set to 1% of the blade length. The blade spacing was set to 20% of the upstream chord [11]. The two turbines can be seen on a smith chart [30], based on the average stage load and flow coefficient for the LPT, in figure 23.

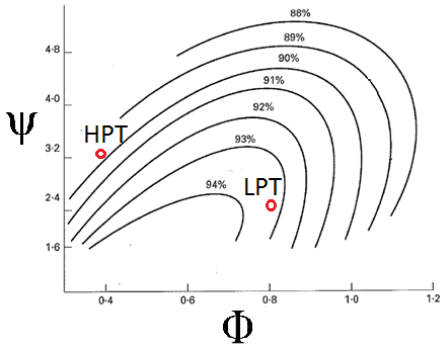

Figure 23: Stage load over flow coefficient for the HPT and LPT

4.3.5.1 HPT

A highly loaded one stage HPT was chosen to minimize the required cooling flow. The HPT inlet area is derived from AN^2 to maintain stress levels based on material technology for 2025. $M_{ax,in}$ was then derived from the area. To avoid high pressure losses in the upstream ducting and to assure that the

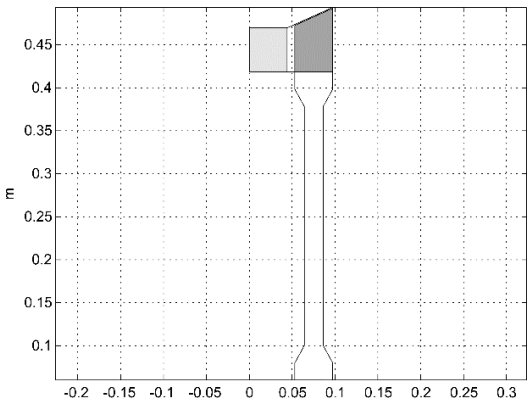

Figure 24: HPT component

gas accelerates at all points along the NGV, it has been kept below 0,2 [11]. The HPT is shown in figure 24. Note that the disc is preliminary, the final disc design can be seen in appendix D.

Some key turbine data can be found in table 11. The velocity triangles for the mean blade can be seen in figure 25 and the corresponding data can be seen in table 12. A full output of stage by stage performance can be seen in appendix C.

$\boldsymbol{AN^2}$	7247,5	***Number of stages***	1
$\boldsymbol{M_{ax,in}}$	0,16	***Stage Temp. drop***	$494K$
$\boldsymbol{M_{ax,out}}$	0,4	$\boldsymbol{\psi}$	3,10
$\boldsymbol{AR_{in}}$	1,16	ϕ	0,41
$\boldsymbol{AR_{out}}$	1,16	$\boldsymbol{\eta_{poly}}$	0.910
$\boldsymbol{\lambda_N}$	0,05	$\boldsymbol{M_{hub,rel}}$	0,35
EIS	2025	***Total length***	$0.097m$

Table 11: Key HPT data

Stage	**1**
$\boldsymbol{\beta_2}$	52
$\boldsymbol{\beta_3}$	68
$\boldsymbol{\alpha_2}$	75
$\boldsymbol{\alpha_3}$	4
$\boldsymbol{C_a}$	259
$\boldsymbol{U}$	630
$\boldsymbol{V_2}$	419
$\boldsymbol{V_3}$	699
$\boldsymbol{C_2}$	994
$\boldsymbol{C_3}$	260
ϕ	0,41
$\boldsymbol{\psi}$	3,10
Deflection	16
Reaction	0,25
$\boldsymbol{M_{hub,rel}}$	0,35
Temp. drop	494

Table 12: HPT velocity triangles data at mean blade

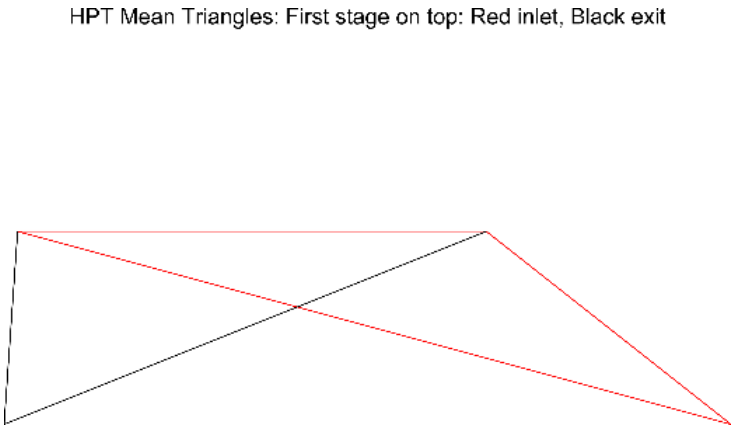

Figure 25: Velocity triangles for the HPT at mean blade

4.3.5.2 LPT

The first stage LPT mean radius was set to correspond with the last stage HPT mean radius in order to achieve a decent stage loading and to approximately align with the fan to reduce flow turning. $M_{ax,out}$ was set high to reduce the rotor outlet area, thus reducing AN^2. Since AN^2 will be lower on the first stage due to the smaller area, calculations are only performed on the second stage. The first stage stator was replaced with an aerodynamically loaded strut to accomplish the same function as a stator, while giving structural support to the engine. With two stages there is no exit swirl entering the LPT exhaust at design point. Some swirl will however be present at off-design conditions. The LPT is shown in figure 26.

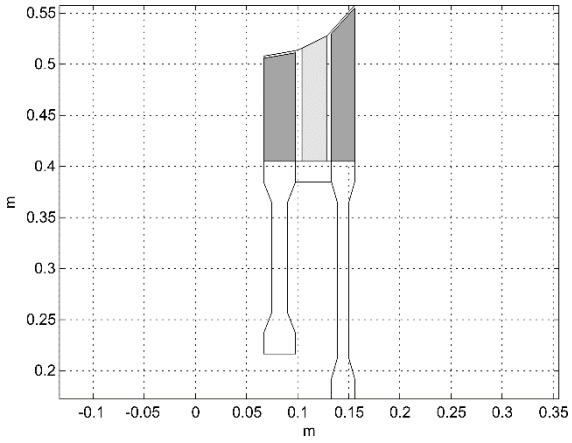

Figure 26: LPT component

Some key turbine data can be found in table 13. The velocity triangles at the mean blade can be seen in figure 27 and the corresponding data can be seen in table 14. A full output of stage by stage performance can be found in appendix C.

$\boldsymbol{M_{ax,in}}$	0,35	$\boldsymbol{Number\ of\ stages}$	2
$\boldsymbol{M_{ax,out}}$	0,5	$\boldsymbol{Avg.\ \psi}$	2,06
$\boldsymbol{AR_{in}}$	1,84	$\boldsymbol{Avg.}\phi$	0,81
$\boldsymbol{AR_{out}}$	6,72	$\boldsymbol{\eta_{poly}}$	0,934
$\boldsymbol{\lambda_N}$	0,05	$\boldsymbol{M_{hub,rel,,stg1}}$	0,40
$\boldsymbol{EIS}$	2025	$\boldsymbol{M_{hub,rel,stg2}}$	0,44
$\boldsymbol{Stage\ Temp.drop}$	$99{,}7K$	$\boldsymbol{Total\ length}$	$0{,}089m$
$\boldsymbol{Last\ stage\ AN^2}$	5115		

Table 13: Key LPT data

$Stage$	**1**	**2**
$\boldsymbol{\beta_2}$	4	0
$\boldsymbol{\beta_3}$	53	49
$\boldsymbol{\alpha_2}$	54	49
$\boldsymbol{\alpha_3}$	0	0
$\boldsymbol{C_a}$	254	295
$\boldsymbol{U}$	335	344
$\boldsymbol{V_2}$	254	295
$\boldsymbol{V_3}$	420	453
$\boldsymbol{C_2}$	435	453
$\boldsymbol{C_3}$	254	295
ϕ	2,11	2,00
$\boldsymbol{\psi}$	0,76	0,86
$\boldsymbol{Deflection}$	49	49
$\boldsymbol{Reaction}$	0,47	0,50
$\boldsymbol{M_{hub,rel}}$	0,40	0,44
$\boldsymbol{Temp.drop}$	100	100

Table 14: LPT velocity triangles data at mean blade

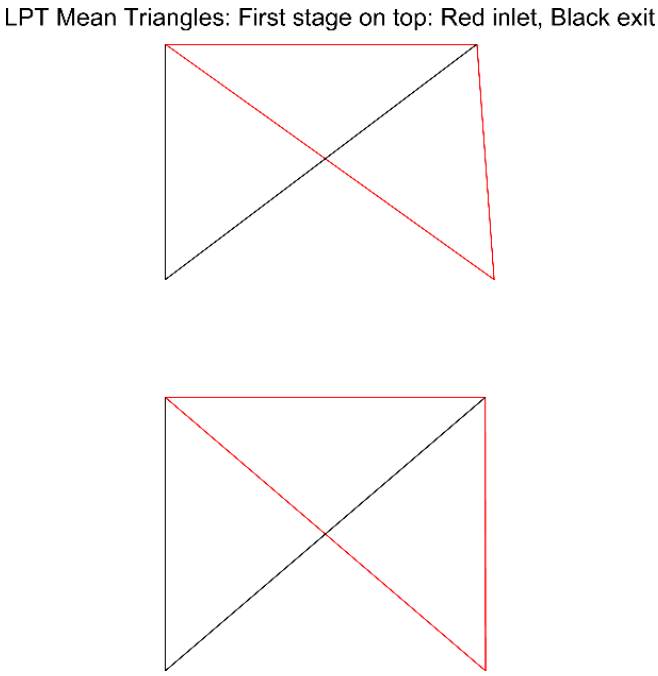

Figure 27: Velocity triangles for the LPT at mean blade

4.3.6 Mixer

The engine uses a lobed annular mixer to improve thrust and SFC and to reduce noise. The mixer length was chosen to attain L/D ~1 to achieve a good percentage of the theoretical thrust gain [11]. The mixer can be seen in figure 28 and the mixer data can be seen in table 15.

$\boldsymbol{Efficiency}$	$0,7$
$\boldsymbol{Cold\ stream\ M}$	$0,552$
$\boldsymbol{Hot\ stream\ M}$	$0,5$
$\boldsymbol{Cold\ stream\ area}$	$0{,}124\ m^2$
$\boldsymbol{Hot\ stream\ area}$	$0{,}461\ m^2$
$\boldsymbol{Length}$	$0{,}2\ m$
$\boldsymbol{L/D}$	1.0767

Table 15: Key mixer data

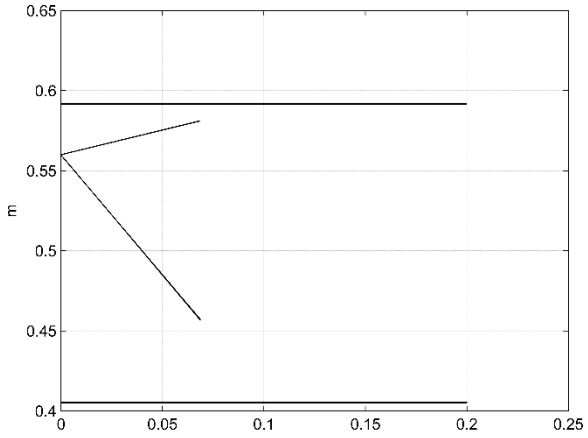

Figure 28: Mixer component

4.3.7 Nozzle

Due to the high nozzle pressure ratio at supersonic speed, a convergent – divergent nozzle was chosen, which can be seen in figure 29. The areas are set to allow for the fluid to fully expand at design point. The angles are a compromise between length and thrust, a lower angle will lead to higher thrust, at the expense of a longer component. For very low angles, the losses due to skin friction will take over. The nozzle data can be seen in table 16. The rate of change in area as a function of distance together with the area as a function of distance in the nozzle can be seen in figure 30.

$\boldsymbol{CV}$	$0,97$
$\boldsymbol{C_\theta}$	$0,988$
$\boldsymbol{Inlet\ area}$	$1,099m^2$
$\boldsymbol{Throat\ area}$	$0,453m^2$
$\boldsymbol{Exit\ area}$	$1,04m^2$
$\boldsymbol{Length}$	1,18m
$\boldsymbol{Divergent\ angle}$	12,5°
$\boldsymbol{Petal\ angle}$	35,2°
$\boldsymbol{PR}$	13,09
$\boldsymbol{A_{th}/A_{out}}$	0,44
$\boldsymbol{A_{in}/A_{th}}$	2,43

Table 16: Key Nozzle data

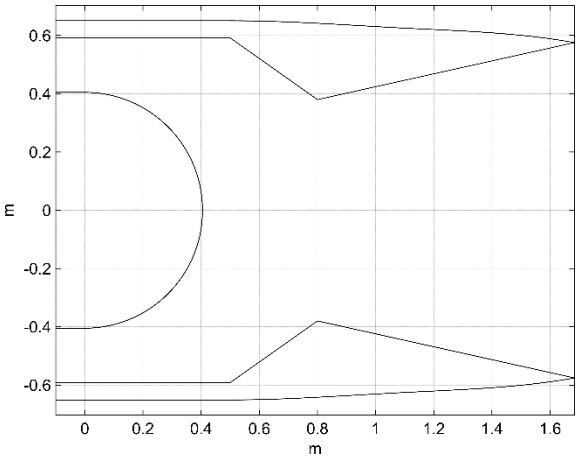

Figure 29: Nozzle component

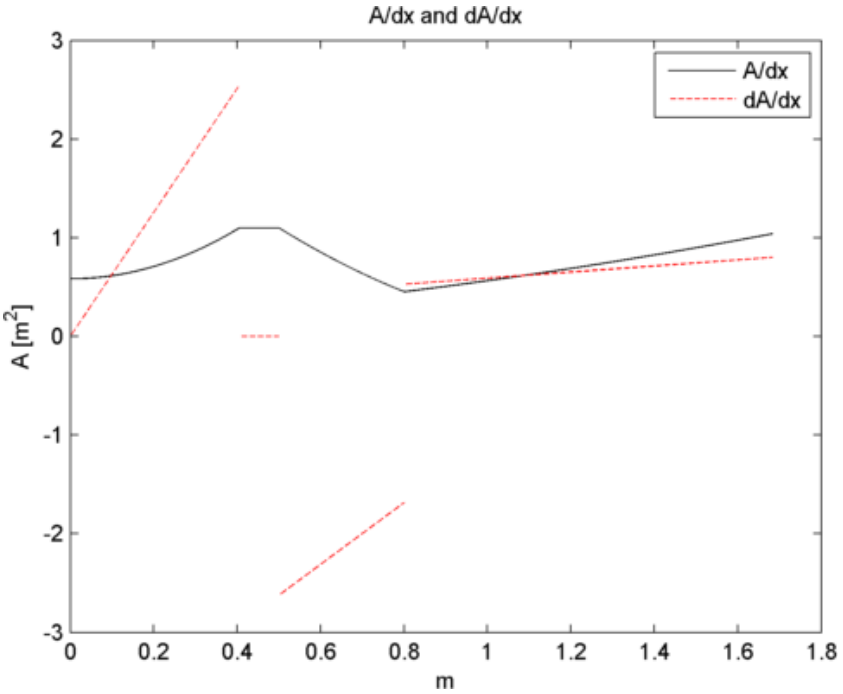

Figure 30: Rate of change in area over distance and area over distance for the nozzle

4.3.8 Discs

The first stage HPC disc with some stress data can be seen in figure 31. The optimum design was a hyperbolic disc with the material Inconel 718. However, the disc had to become very heavy and wide to meet the target safety line due to high rotational speeds, which in turn caused a geometrical problem with the second stage disc. This was solved by making the gap between the center axis of the engine and the inner rim of the disc, also called bore radius, different for the two stages. The first stage has a bore radius of 4cm while the second stage has a bore radius of 9cm.

All the HPC discs, as well as the HPT disc, were designed with a hyperbolic disc and the material Inconel 718, with a bore radius of 4cm, except for the second stage HPC. Table 17 shows some key data for all the discs. The full disc analysis can be found in appendix D.

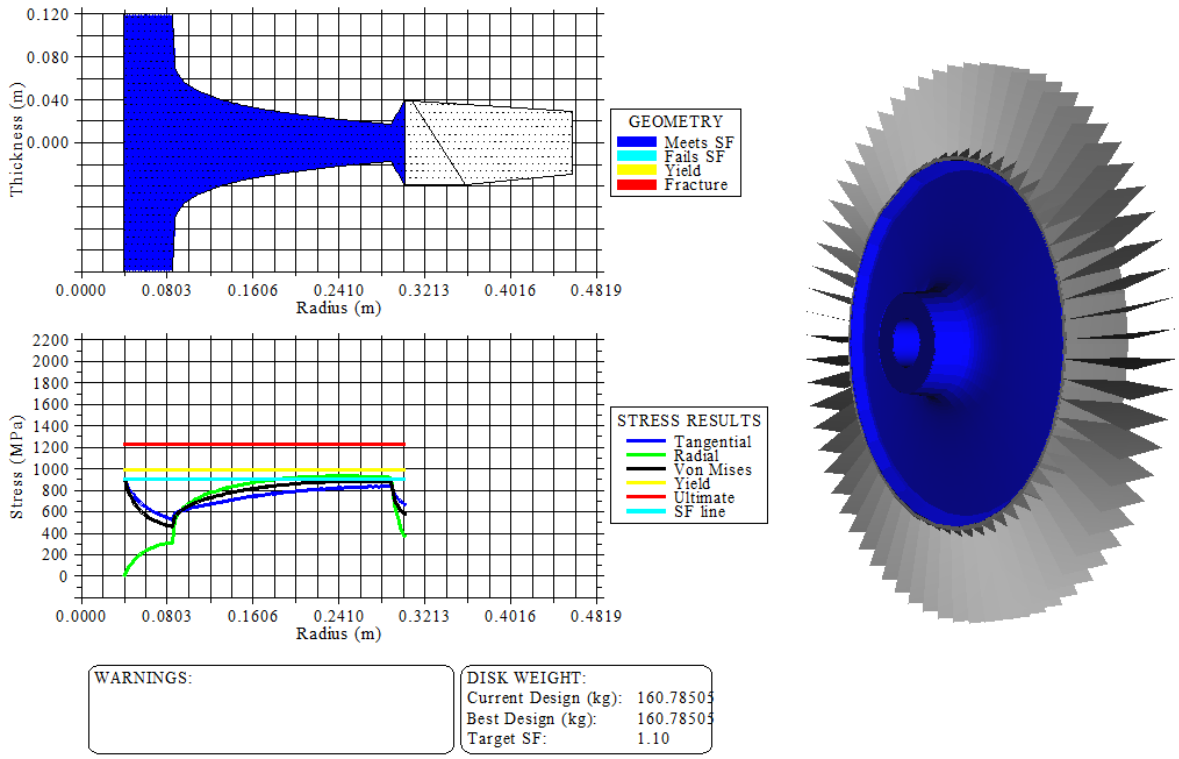

Figure 31: First stage HPC disc output file from T-AXI DISC

Disc	***Weight (kg)***	***Bore radius (cm)***	***Maximun width (cm)***
1^{st} ***HPC***	160,8	4	23,4
2^{nd} ***HPC***	38,3	9	7
3^{rd} ***HPC***	19,8	4	3
4^{th} ***HPC***	16,9	4	2,5
5^{th} ***HPC***	16,9	4	2,4
HPT	104,3	4	16,5

Table 17: Key data for HPC and HPT discs

4.4 Off-design

Figure 32 shows the key operating conditions of a typical mission for the aircraft with the thrust requirements of one engine. Off-design simulations were carried out at these conditions. Some key turbomachinery off-design data can be seen in table 18 – 21. The full off-design performance data can be seen in appendix B.

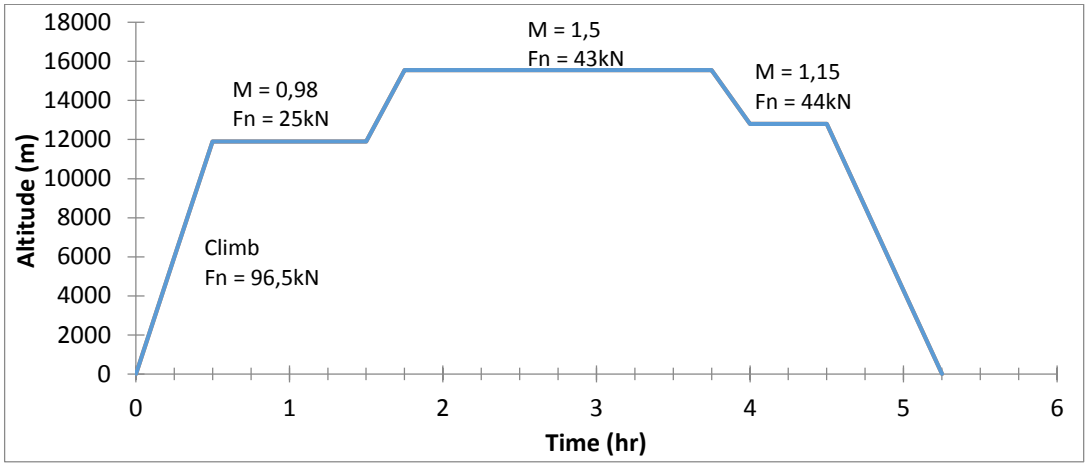

Figure 32: Typical mission for the engine

Component	W_c	***RPM***	η_{poly}
Fan	238	7000	0,901
HPC	54,9	13500	0,941
HPT	14	13500	0,91
LPT	59,9	7000	0,934

Table 18: M 1.5 alt 51000ft

Component	W_c	***RPM***	η_{poly}
Fan	184,6	5542	0,885
HPC	52,2	12204	0,951
HPT	13,7	12204	0,901
LPT	60,9	5542	0,923

Table 19: M 0 alt 0ft

Component	W_c	***RPM***	η_{poly}
Fan	190,6	5348	0,891
HPC	52,5	11622	0,951
HPT	14	11622	0,909
LPT	60,9	5348	0,923

Table 20: M 0,98 alt 38500ft

Component	W_c	***RPM***	η_{poly}
Fan	241,2	6714	0,883
HPC	55,2	12744	0,939
HPT	14	12744	0,91
LPT	59,8	6714	0,935

Table 21: M 1,15 alt 42000ft

4.5 Sensitivity analysis

The purpose of a sensitivity analysis is to investigate the effect that a change in efficiency or pressure loss of a component will have on the efficiency of the engine cycle. This is useful for example when determining whether the cost of developing more efficient components, will pay back in a more efficient engine. Table 22 shows the change in efficiency and pressure loss of certain components and the corresponding change is SFC at design point. Table 23 shows a change in power off-take, HPT blade metal temperature, customer bleed and the corresponding change in SFC at design point.

$\boldsymbol{\Delta Efficiency}$	$\boldsymbol{\Delta SFC}$	$\boldsymbol{\Delta Pressure\ loss}$	$\boldsymbol{\Delta SFC}$
$\boldsymbol{\eta_{poly,fan} + 1\%}$	$-0{,}47\%$	$\boldsymbol{Inlet + 1\%}$	$+0{,}33\%$
$\boldsymbol{\eta_{poly,HPC} + 1\%}$	$-0{,}59\%$	$\boldsymbol{ICD + 1\%}$	$+0.27\%$
$\boldsymbol{\eta_{poly,HPT} + 1\%}$	$-0{,}41\%$	$\boldsymbol{ITD + 1\%}$	$+0.28\%$
$\boldsymbol{\eta_{poly,LPT} + 1\%}$	$-0{,}24\%$	$\boldsymbol{BP\ duct + 1\%}$	$+0{,}06\%$
$\boldsymbol{\eta_{mech,HP-shaft} + 0,5\%}$	-0.49%	$\boldsymbol{LPT\ exhaust + 1\%}$	$+0.28\%$
$\boldsymbol{CV + 1\%}$	$-2{,}52\%$	$\boldsymbol{Jet\ pipe + 1\%}$	$+0.34\%$
$\boldsymbol{C_\theta + 1\%}$	$-2{,}47\%$	$\boldsymbol{Burner + 1\%}$	$+0.28\%$
$\boldsymbol{\eta_{mech,LP-shaft} + 0,5\%}$	-0.24%		

Table 22: Design point exchange rates for efficiencies and pressure losses

$\boldsymbol{\Delta}$	$\boldsymbol{\Delta SFC}$
$\boldsymbol{Power\ off\ take - 100hp}$	$-0{,}24\%$
$\boldsymbol{HPT\ metal\ temp. +10K}$	$-0{,}19\%$
$\boldsymbol{Customer\ bleed\ 3rd\ stage\ HPC\ (high\ power) + 1\%}$	$+2\%$
$\boldsymbol{Customer\ bleed\ 5th\ stage\ HPC\ (low\ power) + 1\%}$	$+2{,}43\%$

Table 23: Design point exchange rates for power off take, HPT metal temp and customer bleed

4.6 Comparison to baseline engine

Table 24 shows a comparison of some key performance parameters for the MJ-Haran S14 and the baseline engine. Table 25 shows the primary contributors of the increased efficiencies. The slight decrease of η_{tran} is due to the higher BPR of the MJ-Haran S14, and the slight decrease in η_{prop} is due to the higher jet velocity, both of these are however very small and are therefore excluded in table 25.

	MJ – Haran S14	**Baseline**	**Difference (%)**
$\boldsymbol{\eta_{core}}$	0,632	0,579	+ 5,3
$\boldsymbol{\eta_{th}}$	0,595	0,546	+ 4,9
$\boldsymbol{\eta_{tran}}$	0,941	0,943	− 0,2
$\boldsymbol{\eta_{prop}}$	0,624	0,625	− 0,1
$\boldsymbol{\eta_{ov}}$	0,371	0,341	+ 3
$\boldsymbol{SFC}(\frac{\boldsymbol{lbm}}{\boldsymbol{hr \cdot lbf}})$	0,981	1,068	− 8,9
$\boldsymbol{Length(m)}$	4,23	4,71	−11,3
$\boldsymbol{Max\ Diameter(m)}$	1,24	1,26	− 1,6

Table 24: Comparison between baseline engine and MJ - Haran S14

	Turbomachinery η increase (%)	**Increase of OPR (%)**	**Increase of TIT (%)**
$\boldsymbol{\eta_{core}}$	+0,8	+2,6	+1,9
$\boldsymbol{\eta_{th}}$	+0,8	+2,8	+1,3
$\boldsymbol{\eta_{ov}}$	+0,5	+1,8	+0,7
$\boldsymbol{SFC}$	−1,5	−4,9	−2,2

Table 25: Primary contributors of increased efficiencies

A weighted fuel flow comparison over the key operating points of a typical mission shows a fuel burn improvement of **11,8%** for the MJ-Haran S14 compared to the baseline engine.

5 Conclusions

In this thesis a preliminary design of a supersonic jet engine for a conceptual business jet expected to enter service in 2025 has been carried out. The engine was expected to provide better performance than that of the current engine chosen to propel the aircraft. Based on the provided engine requirements, the thermodynamic cycle has been optimized and basic sizing and aerodynamic design of the main components has been performed. The result is a shorter engine of similar diameter with improved efficiency. A weighted fuel flow comparison of the two engines at the key operating points shows a fuel burn improvement of 11,8% for the new engine, improving the economic aspects of operating the aircraft and lowering the emissions for a reduced environmental impact.

The design process of a jet engine is a complex process which covers many different disciplines and there is quite often no obvious solution as an improvement of one parameter often comes at the expense of another.

A secondary objective of the thesis was to evaluate whether the knowledge obtained from the courses of the aeronautical program at Mälardalen University are sufficient to perform this type of study, and to recommend courses for students who in the future wish to perform a similar work. The authors' opinion here is that the knowledge obtained is in the lower part of the range of necessary knowledge, but with proper guidance and determination, it's certainly not an impossible task. To cover all parts of the design process within the limits of the program may not be possible. Courses covering: thermodynamics, mechanics, aerodynamics, mathematical programming, computer aided design, aero-engine technology and general mathematics are recommended. Most of these are available in the current curriculum of the program. A course going deeper in the theory of gas turbine technology, with a greater focus on the turbomachinery components, could however be developed to provide a better starting point for a project like this. To follow the method provided in this thesis, good MATLAB skills are necessary.

5.1 Future work

Only the first stages of the conceptual design process have been carried out and some future work is necessary to complete the engine.

- Further off-design analysis need to be performed, including a turbomachinery analysis at the off design points.
- Further mechanical design including material selections, weight estimations and stress calculations need to be carried out.
- A variable geometry inlet and exhaust design may be necessary to assure good performance over the entire flight envelope.

6 References

[1] Dr. I. Halliwell, “Candidate Engines for a Supersonic Business Jet”, Joint AIAA Foundation/ASME.IGTI Student Design Competition 2013/14, Reston, VA, U.S, 2013.

[2] K. G. Kyprianidis, “Future Aero Engine Designs: An Evolving Vision, Advances in Gas Turbine Technology”, InTech, Dr. Ernesto Benini (Ed.), ISBN: 978-953-307-611-9 , doi: 10.5772/19689, 2011

[3] K.G. Kyprianidis, T. Grönstedt, S.O.T. Ogaji, P. Pilidis, R. Singh, “Assessment of Future Aero - engine Designs With Intercooled and Intercooled Recuperated Cores ”, ASME Journal of Engineering for Gas Turbines and Power, Vol. 133, pp. 011701-1 – 011701-10, doi: 10.1115/1.4001982, January, 2011.

[4] T. Lindquist, R. Stieger, M. Hillel,”Recuperated Small Gas Turbines – Recuperator Installation”, SEAS DTC Technical Conference, Edinburgh, UK, 2008.

[5] L. Larsson, T. Grönstedt, K.G. Kyprianidis, “Conceptual Design and Mission Analysis for a Geared Turbofan and an Open Rotor Configuration”, Proceedings of ASME Turbo Expo, GT2011-46451, Vancouver, 2011.

[6] D.P Raymer, “Use of Computers in the Conceptual Design Process”, Aircraft Design Short Course, Dayton, Ohio, 1984.

[7] S.N. Patnaik, D.A Hopkins, “General-purpose optimization method for multidisciplinary design applications”, Advances in Engineering Software 31, pp. 57-63, June, 1999.

[8] P. Jeschke, J. Kurzke, R. Schaber, C. Riegler,”Preliminary Gas Turbine Design Using the Multidisciplinary, Design System MOPEDS”, Journal of Engineering for Gas Turbines and Power, Vol. 126, pp. 258 – 264, April, 2004.

[9] M.J. Jones, S.J. Bradbrook, K. Nurney, “A preliminary Engine Design Process for an Affordable Capability”, RTO-MP-089, Paris, France, 2002.

[10] F. Ersavas, “Multidisciplinary Conceptual Design of a Transonic High Pressure Compressor”, MSc thesis, Chalmers University of Technology, Gothenburg, Sweden, 2011.

[11] P.P. Walsh, P. Fletcher, “Gas Turbine Performance”, Second Edition, Blackwell Science, 2004. ISBN: 0-632-06434-X.

[12] http://www.wolverine-ventures.com/index.php?option=com_content&view=article&id=2&Itemid=2, [20140804].

[13] J. Kurzke, “GasTurb12 – Design and Off-Design Performance of Gas Turbines”, Technical Manual, Germany, 2012.

[14] A. Guha, “Optimum Fan Pressure Ratio for Bypass Engines with Separate or Mixed Exhaust Streams”, Journal of Propulsion and Power, Vol. 17, No. 5, pp. 1117 - 1122, September - October, 2001.

[15] K.G Kyprianidis, “Introduction to Gas Turbine Performance”, Chalmers University of Technology, Gothenburg, Sweden, 2012.

[16] K.G Kyprianidis, MSc course on “Gas Turbine Technology”, Lecture 3, Chalmers University of Technology, Gothenburg, Sweden, 2012.

[17] http://www.mathworks.se/products/matlab, [20140804].

[18] T. Grönstedt, “Conceptual Aero Engine Design modeling – Engine Sizing”, Chalmers University of Technology, Gothenburg, Sweden, 2011.

[19] H.I.H. Saravanamuttoo, C.F.G. Rogers, H. Cohen, P.V. Straznicky,”Gas Turbine Theory”, Sixth Edition, Pearson Prentice Hall, 2009. ISBN: 978-0-13-222437-6.

[20] S.L. Dixon, C.A. Hall, “Fluid Mechanics and Thermodynamics of Turbomachinery” Sixth Edition, Elsevier, 2010. ISBN-13: 978-1856177931.

[21] T. Grönstedt, “Conceptual Aero Engine Design modeling – Efficiency modeling”, Chalmers University of Technology, Gothenburg, Sweden, 2011.

[22] L. Elbrandt, “Conceptual design of an annular combustor for the Whittle engine data”, Chalmers University of Technology, Gothenburg, Sweden, 2011.

[23] K.G Kyprianidis, MSc course on “Gas Turbine Technology”, Lecture 13, Chalmers University of Technology, Gothenburg, Sweden, 2012.

[24] J.D Anderson, Jr.,”Fundamentals of Aerodynamics”, Fifth Edition, McGrawer-Hill Higher Education, 2007. ISBN: 9780071289085.

[25] L.E Stitt,”Exhaust Nozzles for Propulsion Systems with Emphasis on Supersonic Cruise Aircraft”, NASA reference publication 1235, Cleveland, Ohio, 1990.

[26] A. Merchant, D. Bruna, M.G. Turner, “A Turbomachinery Design Tool for Teaching Design Concepts for Axial Flow Fans, Compressors and Turbines”, Proceedings of ASME Turbo Expo, GT2006-90105, Barcelona, 2006.

[27] K.G Kyprianidis, personal communication, 2014

[28] D. Gutzwiller, “T-Axi Disk V2.2 User's Guide and Tutorial”, Cincinnati, Ohio, 2009

[29] K.G Kyprianidis, MSc course on “Gas Turbine Technology”, Lecture 7, Chalmers University of Technology, Gothenburg, Sweden, 2012.

[30] K.G Kyprianidis, MSc course on “Gas Turbine Technology”, Lecture 8, Chalmers University of Technology, Gothenburg, Sweden, 2012.

7 Appendices

A Formulas

Propulsive efficiency

$$\eta_{prop} = \frac{FN \cdot V_0}{W_9 \cdot \frac{V_9^2 - V_0^2}{2}}$$

Thermal efficiency

$$\eta_{th} = \frac{\frac{1}{2} W_9 \cdot V_9^2 - \frac{1}{2} W_0 \cdot V_0^2}{W_f \cdot LHV}$$

Core efficiency

$$\eta_{core} = \frac{\frac{1}{2} W_{47} \cdot V_{47,is}^2 - \frac{1}{2} W_{core} \cdot V_0^2}{W_f \cdot LHV}$$

Transfer efficiency

$$\eta_{trans} = \frac{\eta_{th}}{\eta_{core}}$$

Overall efficiency

$$\eta_{ov} = \eta_{prop} \cdot \eta_{trans} \cdot \eta_{core}$$

Specific fuel consumption

$$SFC = \frac{W_f}{FN}$$

OPR

$$OPR = \frac{P_{03}}{P_{01}}$$

FPR

$$FPR = \frac{P_{021}}{P_{02}}$$

TIT

$$TIT = T_{04}$$

BPR

$$BPR = \frac{W_{13}}{W_{21}}$$

Thrust coefficient

$$CV = \frac{FG}{FG_{con-di,id}}$$

Angularity coefficient

$$C_\theta = \frac{1 + cos(\alpha)}{2}$$

Gross thrust

$$FG = CV[(\, C_\theta \cdot \gamma \cdot P_9 \cdot M_9^2 \cdot A_e) + (P_9 - P_0) \cdot A_9]$$

Stage loading

$$\psi = \frac{\Delta h}{U^2}$$

Corrected mass flow

$$W_c = W \sqrt{\frac{T_0}{T_{std}}} \Big/ \frac{P_0}{P_{std}}$$

Flow coefficient

$$\Phi = \frac{C_x}{U}$$

Degree of reaction

$$R = \frac{h_2 - h_1}{h_{02} - h_{01}}$$

De Haller number

$$deHaller = \frac{V_2}{V_1}$$

Diffusion factor

$$DF = 1 - \frac{V_2}{V_1} + \frac{\Delta C_w}{2V_1} \cdot \frac{s}{c}$$

Deflection

$$\varepsilon = \alpha_1 - \alpha_2$$

Combustor loading

$$Loading = \frac{W_{in}}{V_L \cdot P_{o,in}^{1.8} \cdot 10^{0.00145(T_{0,in}-400)}}$$

Residence time

$$\tau_{res} = \frac{L_L}{C_L}$$

B NPSS outputs

Design point

(All values are in imperial units)

Summary Output Data

MN	alt	W	Fg	Fn	SFC	Wfuel	WAR	OPR	BPR	FPR	SFn
1.500	51000.0	198.0	18495.1	9555.0	0.9807	9370.76	0.0000	38.000	0.40	3.93	48.26

ETA,core	ETA,prop	ETA,tran	ETA,th	Vbp/Vcore	%CoolFlow
0.6324	0.624	0.941	0.595	0.80	16.2

INPUT FLOW

		W	Pt	Tt	ht	FAR	wc	Ps	Ts	Aphy	MN	gamt
FS0	Inlet.Fl_I	198.00	5.887	565.90	135.28	0.0000	516.28	1.603	389.97	1768.9	1.5000	1.39961
FS1	Fan.Fl_I	198.00	5.789	565.89	135.28	0.0000	524.98	4.359	521.78	0.0	0.6500	1.39961
FS2	Splitter.F>	198.00	22.741	870.15	208.95	0.0000	165.73	0.000	0.00	0.0	0.0000	1.38855
FS13	DuctBP.Fl_I	56.27	22.741	870.15	208.95	0.0000	47.10	0.000	0.00	0.0	0.0000	1.38855
FS22	DuctSplit.>	141.73	22.741	870.15	208.95	0.0000	118.63	0.000	0.00	0.0	0.0000	1.38855
FS25	HPC.Fl_I	141.73	22.286	870.15	208.95	0.0000	121.05	0.000	0.00	0.0	0.0000	1.38855
FS3	Burner.Fl_I	118.74	223.710	1678.41	416.78	0.0000	14.03	0.000	0.00	0.0	0.0000	1.34150
Blc	HPT.Bl_I2	9.20	223.710	1678.41	416.78	0.0000	10.92	0.000	0.00	0.0	0.0000	1.34150
FS4	HPT.Fl_I	121.34	214.538	2959.94	802.63	0.0219	19.86	0.000	0.00	0.0	0.0000	1.28992
NGVc	HPT.Bl_I1	13.79	223.710	1678.41	416.78	0.0000	16.36	0.000	0.00	0.0	0.0000	1.34150
FS44	DuctIT.Fl_I	144.33	50.735	2070.46	535.57	0.0184	83.53	0.000	0.00	0.0	0.0000	1.31278
FS45	LPT.Fl_I	144.33	49.720	2070.46	535.57	0.0184	85.23	0.000	0.00	0.0	0.0000	1.31278
FS5	DuctPreMix>	144.33	21.436	1711.68	434.00	0.0184	179.75	0.000	0.00	0.0	0.0000	1.32706
FS163	Mixer.Fl_I2	56.27	22.059	870.15	208.95	0.0000	48.56	17.937	821.12	177.4	0.5533	1.38855
FS63	Mixer.Fl_I1	144.33	21.115	1711.68	434.00	0.0184	182.49	17.937	1644.05	728.5	0.5000	1.32706
FS7	JetPipe.Fl>	200.60	21.196	1488.55	370.87	0.0131	235.63	17.700	1421.50	905.9	0.5237	1.34169
FS8	Nozzle.Fl_I	200.60	20.984	1488.55	370.87	0.0131	238.01	0.000	0.00	0.0	0.0000	1.34169
FS9	Fl_end.Fl_I	200.60	20.984	1488.55	370.87	0.0131	238.01	1.603	746.90	1614.1	2.3170	1.34169

INLETS

	eRam	Afs	Fram
Inlet	0.9834	1768.88	8940.1

DUCTS

	dPqP	MNin	Aphy
DuctBP	0.03000	0.0000	0.00
DuctSplit	0.02000	0.0000	0.00
DuctIT	0.02000	0.0000	0.00
DuctPreMix	0.01500	0.0000	0.00
JetPipe	0.01000	0.5237	905.88

SPLITTERS

	BPR	dP/P1	dP/P2
Splitter	0.39705	0.0000	0.0000

MIXERS

	%mix	des	MN1	MN2	A1	A2	Ps1	Ps2
Mixer	0.70	1	0.500	0.553	728.5	177.4	17.937	17.937

BURNERS

	TtOut	eff	dPqP	Wfuel	FAR
Burner	2960.00	0.9999	0.0410	2.60299	0.02192

NOZZLES

	PR	Cfg	CdTh	Cv	Ath	Vactual	Fg
Nozzle	13.090	0.96	1.00	0.97	702.74	2966.4	18495.1

SHAFTS

	Nmech	trqIn	trqNet	pwrIn	HPX	dNqdt
HP_SHAFT	13500.0	16333.8	-0.0123	41984.3	100.00	0.00
LP_SHAFT	7000.0	15561.8	0.0073	20740.7	0.00	0.00

COMPRESSORS & TURBINES

	Wc|Wp	PR	TR	effPoly	eff	Nc|Np	pwr
Fan	524.98	3.928	1.5377	0.9010	0.8808	6701.6	-20636.9
HPC	121.05	10.038	1.9289	0.9410	0.9214	10422.7	-41674.4
HPT	30.77	4.229	1.3513	0.9100	0.9229	248.1	41984.3
LPT	132.09	2.319	1.2096	0.9340	0.9402	153.8	20740.7

MAP POINTS - COMPRESSORS & TURBINES

	Wc|WpMap	PRmap	effMap	Nc|NpMap	Rline
Fan	1441.71	1.677	0.8703	1.000	2.0000
HPC	123.57	24.136	0.8216	1.000	2.0000
HPT	15.77	4.975	0.9220	100.000	
LPT	78.56	4.271		0.9171	100.000

ADDERS AND SCALARS

	s_Wc|WpAud	a_Wc|WpAud	s_PRaud	a_PRaud	s_effAud	a_effAud
Fan	1.0000	0.0000	1.0000	0.0000	1.0000	0.0000
HPC	1.0000	0.0000	1.0000	0.0000	1.0000	0.0000
HPT	1.0000	0.0000	1.0000	0.0000	1.0000	0.0000
LPT	1.0000	0.0000	1.0000	0.0000	1.0000	0.0000

BLEEDS

		Wb/Win	dhb/dh	dPb/dP	Tt	ht
Blc	HPC.Bl_cool2	0.0649	1.0000	0.0000	1678.41	416.78
NGVc	HPC.Bl_cool1	0.0973	1.0000	0.0000	1678.41	416.78

Off design

Summary Output Data

MN	alt	W	Fg	Fn	SFC	wfuel	WAR	OPR	BPR	FPR	SFn
0.000	0.0	400.6	21699.8	21699.8	0.5821	12631.97	0.0000	26.087	0.46	2.95	54.17

ETA,core	ETA,prop	ETA,tran	ETA,th	Vbp/Vcore	%CoolFlow
0.4293	0.000	0.926	0.398	0.99	16.2

INPUT FLOW

		W	Pt	Tt	ht	FAR	Wc	Ps	Ts	Aphy	MN	gamt
FS0	Inlet.Fl_I	400.64	14.696	518.67	123.95	0.0000	400.64	14.696	518.67	-----.-	0.0000	1.40052
FS1	Fan.Fl_I	400.64	14.452	518.67	123.95	0.0000	407.40	12.621	498.95	1737.1	0.4441	1.40052
FS2	Splitter.F>	400.64	42.595	734.56	175.93	0.0000	164.50	0.000	0.00	0.0	0.0000	1.39485
FS13	DuctBP.Fl_I	126.04	42.595	734.56	175.93	0.0000	51.75	0.000	0.00	0.0	0.0000	1.39485
FS22	DuctSplit.>	274.60	42.595	734.56	175.93	0.0000	112.75	0.000	0.00	0.0	0.0000	1.39485
FS25	HPC.Fl_I	274.60	41.743	734.56	175.93	0.0000	115.05	0.000	0.00	0.0	0.0000	1.39485
FS3	Burner.Fl_I	230.06	383.374	1392.96	341.07	0.0000	14.45	0.000	0.00	0.0	0.0000	1.35631
Blc	HPT.Bl_I2	17.83	383.374	1392.96	341.07	0.0000	10.29	0.000	0.00	0.0	0.0000	1.35631
FS4	HPT.Fl_I	233.56	367.656	2342.88	612.43	0.0153	19.84	0.000	0.00	0.0	0.0000	1.30715
NGVc	HPT.Bl_I1	26.71	383.374	1392.96	341.07	0.0000	15.41	0.000	0.00	0.0	0.0000	1.35631
FS44	DuctIT.Fl_I	278.11	84.877	1614.37	404.83	0.0128	84.95	0.000	0.00	0.0	0.0000	1.33547
FS45	LPT.Fl_I	278.11	83.179	1614.37	404.83	0.0128	86.69	0.000	0.00	0.0	0.0000	1.33547
FS5	DuctPreMix>	278.11	37.048	1334.10	329.58	0.0128	176.93	0.000	0.00	0.0	0.0000	1.35088
FS163	Mixer.Fl_I2	126.04	41.318	734.56	175.93	0.0000	53.35	31.237	678.55	177.4	0.6456	1.39485
FS63	Mixer.Fl_I1	278.11	36.492	1334.10	329.58	0.0128	179.62	31.238	1281.13	728.5	0.4840	1.35088
FS7	JetPipe.Fl>	404.15	37.353	1153.93	281.66	0.0088	237.17	31.115	1098.72	905.9	0.5232	1.36493
FS8	Nozzle.Fl_I	404.15	36.980	1153.93	281.66	0.0088	239.56	0.000	0.00	0.0	0.0000	1.36493
FS9	Fl_end.Fl_I	404.15	36.980	1153.93	281.66	0.0088	239.56	14.696	897.77	732.2	1.2331	1.36493

INLETS

	eRam	Afs	Fram
Inlet	0.9834	----.--	0.0

DUCTS

	dPqP	MNin	Aphy
DuctBP	0.03000	0.0000	0.00
DuctSplit	0.02000	0.0000	0.00
DuctIT	0.02000	0.0000	0.00
DuctPreMix	0.01500	0.0000	0.00
JetPipe	0.01000	0.5232	905.88

SPLITTERS

	BPR	dP/P1	dP/P2
Splitter	0.45900	0.0000	0.0000

MIXERS

	%mix	des	MN1	MN2	A1	A2	Ps1	Ps2
Mixer	0.70	1	0.484	0.646	728.5	177.4	31.238	31.237

BURNERS

	TtOut	eff	dPqP	Wfuel	FAR
Burner	2342.86	0.9999	0.0410	3.50888	0.01525

NOZZLES

	PR	Cfg	CdTh	Cv	Ath	Vactual	Fg
Nozzle	2.516	0.96	1.00	0.97	702.74	1727.5	21699.8

SHAFTS

	Nmech	trqIn	trqNet	pwrIn	HPX	dNqdt
HP_SHAFT	12204.1	27793.9	-0.3491	64583.4	100.00	0.00
LP_SHAFT	5542.9	28056.0	-0.4209	29609.6	0.00	0.00

COMPRESSORS & TURBINES

	Wc|Wp	PR	TR	effPoly	eff	Nc|Np	pwr
Fan	407.40	2.947	1.4162	0.8849	0.8664	5543.0	-29462.0
HPC	115.05	9.184	1.8963	0.9509	0.9347	10255.0	-64161.3
HPT	30.75	4.332	1.3787	0.9088	0.9229	252.1	64583.4
LPT	134.34	2.245	1.2101	0.9228	0.9300	138.0	29609.6

MAP POINTS - COMPRESSORS & TURBINES

	Wc|WpMap	PRmap	effMap	Nc|NpMap	Rline
Fan	1118.80	1.450	0.8561	0.827	1.3862
HPC	117.44	21.950	0.8335	0.984	2.1069
HPT	15.75	5.102	0.9220	101.610	
LPT	79.90	4.087	0.9071	89.676	

ADDERS AND SCALARS

	s_Wc|wpAud	a_Wc|WpAud	s_PRaud	a_PRaud	s_effAud	a_effAud
Fan	1.0000	0.0000	1.0000	0.0000	1.0000	0.0000
HPC	1.0000	0.0000	1.0000	0.0000	1.0000	0.0000
HPT	1.0000	0.0000	1.0000	0.0000	1.0000	0.0000
LPT	1.0000	0.0000	1.0000	0.0000	1.0000	0.0000

BLEEDS

		Wb/Win	dhb/dh	dPb/dP	Tt	ht
Blc	HPC.Bl_cool2	0.0649	1.0000	0.0000	1392.96	341.07
NGVc	HPC.Bl_cool1	0.0973	1.0000	0.0000	1392.96	341.07

****

Summary Output Data

MN	alt	W	Fg	Fn	SFC	wfuel	WAR	OPR	BPR	FPR	SFn
0.980	38500.0	160.6	10356.6	5619.9	0.8206	4611.79	0.0000	27.282	0.45	3.04	35.00

ETA,core	ETA,prop	ETA,tran	ETA,th	Vbp/Vcore	%CoolFlow
0.5268	0.584	0.941	0.496	0.97	16.2

INPUT FLOW

		W	Pt	Tt	ht	FAR	Wc	Ps	Ts	Aphy	MN	gamt
FS0	Inlet.Fl_I	160.57	5.409	465.12	111.13	0.0000	413.16	2.923	389.97	1204.0	0.9800	1.40124
FS1	Fan.Fl_I	160.57	5.319	465.12	111.13	0.0000	420.12	4.593	446.00	1737.1	0.4623	1.40124
FS2	Splitter.F>	160.57	16.189	664.50	159.00	0.0000	164.98	0.000	0.00	0.0	0.0000	1.39728
FS13	DuctBP.Fl_I	50.21	16.189	664.50	159.00	0.0000	51.59	0.000	0.00	0.0	0.0000	1.39728
FS22	DuctSplit.>	110.36	16.189	664.50	159.00	0.0000	113.39	0.000	0.00	0.0	0.0000	1.39728
FS25	HPC.Fl_I	110.36	15.866	664.50	159.00	0.0000	115.71	0.000	0.00	0.0	0.0000	1.39728
FS3	Burner.Fl_I	92.46	147.554	1273.39	310.10	0.0000	14.43	0.000	0.00	0.0	0.0000	1.36354
Blc	HPT.Bl_I2	7.17	147.554	1273.39	310.10	0.0000	10.40	0.000	0.00	0.0	0.0000	1.36354
FS4	HPT.Fl_I	93.74	141.505	2156.05	557.36	0.0139	19.85	0.000	0.00	0.0	0.0000	1.31320
NGVc	HPT.Bl_I1	10.74	147.554	1273.39	310.10	0.0000	15.58	0.000	0.00	0.0	0.0000	1.36354
FS44	DuctIT.Fl_I	111.64	32.610	1476.01	366.96	0.0116	84.87	0.000	0.00	0.0	0.0000	1.34342
FS45	LPT.Fl_I	111.64	31.958	1476.01	366.96	0.0116	86.61	0.000	0.00	0.0	0.0000	1.34342
FS5	DuctPreMix>	111.64	14.141	1213.71	297.77	0.0116	177.48	0.000	0.00	0.0	0.0000	1.35920
FS163	Mixer.Fl_I2	50.21	15.704	664.50	159.00	0.0000	53.18	11.911	614.20	177.4	0.6412	1.39728
FS63	Mixer.Fl_I1	111.64	13.929	1213.71	297.77	0.0116	180.18	11.911	1164.37	728.5	0.4844	1.35920
FS7	JetPipe.Fl>	161.85	14.244	1048.73	254.72	0.0080	237.45	11.861	997.77	905.9	0.5224	1.37218
FS8	Nozzle.Fl_I	161.85	14.102	1048.73	254.72	0.0080	239.84	0.000	0.00	0.0	0.0000	1.37218
FS9	Fl_end.Fl_I	161.85	14.102	1048.73	254.72	0.0080	239.84	2.923	677.85	933.9	1.6845	1.37218

INLETS

	eRam	Afs	Fram
Inlet	0.9834	1204.03	4736.7

DUCTS

	dPqP	MNin	Aphy
DuctBP	0.03000	0.0000	0.00
DuctSplit	0.02000	0.0000	0.00
DuctIT	0.02000	0.0000	0.00
DuctPreMix	0.01500	0.0000	0.00
JetPipe	0.01000	0.5224	905.88

SPLITTERS

	BPR	dP/P1	dP/P2
Splitter	0.45495	0.0000	0.0000

MIXERS

	%mix	des	MN1	MN2	A1	A2	Ps1	Ps2
Mixer	0.70	1	0.484	0.641	728.5	177.4	11.911	11.911

BURNERS

	TtOut	eff	dPqP	Wfuel	FAR
Burner	2156.03	0.9999	0.0410	1.28105	0.01386

NOZZLES

	PR	Cfg	CdTh	Cv	Ath	Vactual	Fg
Nozzle	4.824	0.96	1.00	0.97	702.74	2058.8	10356.6

SHAFTS

	Nmech	trqIn	trqNet	pwrIn	HPX	dNqdt
HP_SHAFT	11621.8	10761.3	0.0488	23812.5	100.00	0.00
LP_SHAFT	5347.6	10734.5	-0.4088	10929.7	0.00	0.00

COMPRESSORS & TURBINES

	Wc|Wp	PR	TR	effPoly	eff	Nc|Np	pwr
Fan	420.12	3.044	1.4286	0.8912	0.8731	5647.1	-10875.5
HPC	115.71	9.300	1.9163	0.9505	0.9339	10267.7	-23593.4
HPT	30.76	4.339	1.3869	0.9087	0.9229	250.3	23812.5
LPT	134.21	2.260	1.2161	0.9234	0.9308	139.2	10929.7

MAP POINTS - COMPRESSORS & TURBINES

	Wc|WpMap	PRmap	effMap	Nc|NpMap	Rline
Fan	1153.67	1.473	0.8626	0.843	1.4285
HPC	118.11	22.247	0.8327	0.985	2.0799
HPT	15.76	5.111	0.9221	100.868	
LPT	79.83	4.123	0.9079	90.480	

ADDERS AND SCALARS

	s_Wc|wpAud	a_Wc|WpAud	s_PRaud	a_PRaud	s_effAud	a_effAud
Fan	1.0000	0.0000	1.0000	0.0000	1.0000	0.0000
HPC	1.0000	0.0000	1.0000	0.0000	1.0000	0.0000
HPT	1.0000	0.0000	1.0000	0.0000	1.0000	0.0000
LPT	1.0000	0.0000	1.0000	0.0000	1.0000	0.0000

BLEEDS

		Wb/Win	dhb/dh	dPb/dP	Tt	ht
Blc	HPC.Bl_cool2	0.0649	1.0000	0.0000	1273.39	310.10
NGVc	HPC.Bl_cool1	0.0973	1.0000	0.0000	1273.39	310.10

Summary Output Data

MN	alt	W	Fg	Fn	SFC	Wfuel	WAR	OPR	BPR	FPR	SFn
1.150	42000.0	205.0	16797.9	9699.9	0.8892	8624.95	0.0000	39.208	0.39	4.00	47.31

ETA,core	ETA,prop	ETA,tran	ETA,th	Vbp/Vcore	%CoolFlow
0.5887	0.565	0.944	0.556	0.79	16.2

INPUT FLOW

		W	Pt	Tt	ht	FAR	Wc	Ps	Ts	Aphy	MN	gamt
FS0	Inlet.Fl_I	205.04	5.620	493.45	117.91	0.0000	523.01	2.471	389.97	1550.3	1.1500	1.40092
FS1	Fan.Fl_I	205.04	5.527	493.45	117.91	0.0000	531.83	4.103	453.10	1737.1	0.6662	1.40092
FS2	Splitter.F>	205.04	22.100	771.40	184.86	0.0000	166.28	0.000	0.00	0.0	0.0000	1.39333
FS13	DuctBP.Fl_I	57.94	22.100	771.40	184.86	0.0000	46.99	0.000	0.00	0.0	0.0000	1.39333
FS22	DuctSplit.>	147.11	22.100	771.40	184.86	0.0000	119.30	0.000	0.00	0.0	0.0000	1.39333
FS25	HPC.Fl_I	147.11	21.658	771.40	184.86	0.0000	121.73	0.000	0.00	0.0	0.0000	1.39333
FS3	Burner.Fl_I	123.24	220.335	1510.73	372.02	0.0000	14.03	0.000	0.00	0.0	0.0000	1.34978
Blc	HPT.Bl_I2	9.55	220.335	1510.73	372.02	0.0000	11.06	0.000	0.00	0.0	0.0000	1.34978
FS4	HPT.Fl_I	125.64	211.301	2681.00	715.86	0.0194	19.87	0.000	0.00	0.0	0.0000	1.29662
NGVc	HPT.Bl_I1	14.31	220.335	1510.73	372.02	0.0000	16.57	0.000	0.00	0.0	0.0000	1.34978
FS44	DuctIT.Fl_I	149.50	49.957	1863.22	475.42	0.0163	83.35	0.000	0.00	0.0	0.0000	1.32183
FS45	LPT.Fl_I	149.50	48.958	1863.22	475.42	0.0163	85.06	0.000	0.00	0.0	0.0000	1.32183
FS5	DuctPreMix>	149.50	20.900	1529.71	383.14	0.0163	180.53	0.000	0.00	0.0	0.0000	1.33739
FS163	Mixer.Fl_I2	57.94	21.437	771.40	184.86	0.0000	48.44	17.462	727.93	177.4	0.5502	1.39333
FS63	Mixer.Fl_I1	149.50	20.586	1529.71	383.14	0.0163	183.28	17.463	1467.29	728.5	0.5006	1.33739
FS7	JetPipe.Fl>	207.44	20.655	1328.39	327.76	0.0117	236.20	17.233	1266.97	905.9	0.5231	1.35197
FS8	Nozzle.Fl_I	207.44	20.448	1328.39	327.76	0.0117	238.59	0.000	0.00	0.0	0.0000	1.35197
FS9	Fl_end.Fl_I	207.44	20.448	1328.39	327.76	0.0117	238.59	2.471	749.34	1237.1	2.0312	1.35197

INLETS

	eRam	Afs	Fram
Inlet	0.9834	1550.28	7098.0

DUCTS

	dPqP	MNin	Aphy
DuctBP	0.03000	0.0000	0.00
DuctSplit	0.02000	0.0000	0.00
DuctIT	0.02000	0.0000	0.00
DuctPreMix	0.01500	0.0000	0.00
JetPipe	0.01000	0.5231	905.88

SPLITTERS

	BPR	dP/P1	dP/P2
Splitter	0.39386	0.0000	0.0000

MIXERS

	%mix	des	MN1	MN2	A1	A2	Ps1	Ps2
Mixer	0.70	1	0.501	0.550	728.5	177.4	17.463	17.462

BURNERS

	TtOut	eff	dPqP	Wfuel	FAR
Burner	2681.06	0.9999	0.0410	2.39582	0.01944

NOZZLES

	PR	Cfg	CdTh	Cv	Ath	Vactual	Fg
Nozzle	8.276	0.96	1.00	0.97	702.74	2605.4	16797.9

SHAFTS

	Nmech	trqIn	trqNet	pwrIn	HPX	dNqdt
HP_SHAFT	12744.0	16175.5	-0.0423	39249.1	100.00	0.00
LP_SHAFT	6714.3	15270.0	0.0347	19521.3	0.00	0.00

INERTIA

	inertia	inertiaSum
HP_SHAFT	0.00	0.00
LP_SHAFT	0.00	0.00
Fan	0.00	
HPC	0.00	
HPT	0.00	
LPT	0.00	

COMPRESSORS & TURBINES

	Wc|Wp	PR	TR	effPoly	eff	Nc|Np	pwr
Fan	531.83	3.999	1.5633	0.8834	0.8593	6883.8	-19423.6
HPC	121.73	10.173	1.9584	0.9391	0.9184	10449.9	-38953.0
HPT	30.79	4.230	1.3591	0.9095	0.9229	246.1	39249.1
LPT	131.81	2.343	1.2180	0.9346	0.9408	155.5	19521.3

MAP POINTS - COMPRESSORS & TURBINES

	Wc|WpMap	PRmap	effMap	Nc|NpMap	Rline
Fan	1460.45	1.693	0.8490	1.027	2.0251
HPC	124.26	24.482	0.8189	1.003	1.9710
HPT	15.77	4.976	0.9220	99.189	
LPT	78.40	4.328	0.9177	101.113	

ADDERS AND SCALARS

	s_Wc|WpAud	a_Wc|WpAud	s_PRaud	a_PRaud	s_effAud	a_effAud
Fan	1.0000	0.0000	1.0000	0.0000	1.0000	0.0000
HPC	1.0000	0.0000	1.0000	0.0000	1.0000	0.0000
HPT	1.0000	0.0000	1.0000	0.0000	1.0000	0.0000
LPT	1.0000	0.0000	1.0000	0.0000	1.0000	0.0000

BLEEDS

		wb/win	dhb/dh	dPb/dP	Tt	ht
Blc	HPC.Bl_cool2	0.0649	1.0000	0.0000	1510.73	372.02
NGVc	HPC.Bl_cool1	0.0973	1.0000	0.0000	1510.73	372.02

C MATLAB program output files

```
-----------------------------FAN-------------------------------
Entry Into Service:                  2025
Stages:                              4
Av. Stage loading 2dH/Umid2:         1.0223
1st stage Flow coefficient Cax/Umid: 0.76598
1st stage Mtip,rel:                  1.4837
1st stage Utip,in:                   455.1531
1st stage Utip,in,corr:              435.7497
1st stage Umid,in:                   289.5909
1st stage Cax,in:                    221.8209
1st stage Hade angle:                21
(rhub/rtip)in:                       0.2725
(rhub/rtip)out:                      0.69474
AR,in                                2.4
AR,out                               2.3
M,ax,in                              0.65
M,ax,in                              0.38
Total length [m]:                    0.9876
RNI:                                 0.35315
Mcorr:                               238.1475
dETAEIS:                             0.016354
dETARe:                              -0.012639
dETAM:                               0
ETA*:                                0.89693
ETApol:                              0.90065
-----------------------------HPC-------------------------------
Stages:                              5
1:st stg Flow function HPC:          0.42313
Avg. Stage load HPC:                 0.7074
1:st stg(hub/tip)-ratio:             0.70373
last stg(hub/tip)-ratio:             0.94776
1:st stg Mtip,rel no IGV:            1.5247
AR,in                                1.6325
AR,out                               0.9325
M,ax,in                              0.517
M,ax,in                              0.329
Total length [m]:                    0.37088
RNI:                                 0.80258
Mcorr:                               54.9092
dETAEIS:                             0.018391
dETARe:                              -0.0021124
dETAM:                               -0.0014644
ETA*:                                0.9258
ETApol:                              0.94062
---------------------------Combustor-----------------------------
At Cruise conditions
Pattern Factor:                      0.35259
dp:                                  4.1152
burning time:                        0.004021
Vcc [m^3]:                           0.058889
Vcc [m^3]:                           0.029445
Total length [m]:                    0.195
At windmilling conditions
Loading:                             230.9597
```

```
------------------------------HPT-------------------------------
Stages:                                 1
1:st stg Flow function HPT:             0.41448
Avg. Stage load HPT:                    3.1288
AN2:                                    7247.5
AR,in                                   1.16
AR,out                                  1.16
M,ax,in                                 0.15852
M,ax,in                                 0.4
Total length [m]:                       0.097334
RNI:                                    1.822
Mcorr:                                  9.0066
dETAEIS:                                0.0084819
dETARe:                                 0.0056299
dETAM:                                  -0.034234
ETA*:                                   0.95693
ETApol:                                 0.9099
------------------------------LPT-------------------------------
Stages:                                 2
1:st stg Flow function LPT:             0.75935
Avg. Stage load LPT:                    2.1106
Last stg AN2:                           5114.8347
AR,in                                   1.835
AR,out                                  6.7225
M,ax,in                                 0.35
M,ax,in                                 0.5
Total length [m]:                       0.089104
RNI:                                    0.64113
Mcorr:                                  38.6614
dETAEIS:                                0.016457
dETARe:                                 -0.0045817
dETAM:                                  -0.0082715
ETA*:                                   0.93012
ETApol:                                 0.93372
------------------------------Engine----------------------------
OPR:                                    38.0
BPR:                                    0.39702
FPR:                                    3.9283
HPC P-ratio:                            10.0381
Inlet Diameter [m]:                     1.2418
Inlet Area [m]:                         1.2112
Engine Length [m]:                      4.2305
Core length: FANstart-LPTend [m]:       2.0971
LowSpeedShaft [rps]:                    116.6667
HighSpeedShaft [rps]:                   225
------------------------------Ducts-----------------------------
ICD length [m]:                         0.14886
ITD length [m]:                         0.1067
LPT exhaust length [m]:                 0.15
BP duct length [m]:                     1.1627
Jet pipe length [m]:                    0.5
Mixer length [m]                        0.2
------------------------------Nozzle----------------------------
Nozzle length [m]                       1.1834
Petal angle [deg]:                      35.2059
Divergent angle [deg]:                  12.5
Throat Diameter [m]:                    0.75978
Exit Diameter [m]:                      1.1515
```

Ain/Athroat:	2.4249
Athroat/Aexit:	0.43538
Athroat:	0.45338
Aexit:	1.0414
Ain:	1.0994

----------Inlet----------

Total Pressure recovery Inlet:	0.98342
Total length Inlet:	2.0884
Total Engine length with Inlet:	6.3189
Venturi Area [m^2]:	0.99211
Oblique shock angle "beta" [deg]:	55
Deflection angle "theta" [deg]:	9.2563
Mach number after oblique shock:	1.1517
Mach number after normal shock:	0.87387
Mach number inlet FAN:	0.65

----------Velocity Diagram FAN----------

Mtip,rel:	1.4297
Average Stage Load:	0.81845
Average Flow coefficient:	0.62704
Average Temp rise:	42.2583

	Stage	Hubradii	Midradii	Tipradii
beta1	1	51.128	52.549	63.069
beta2	1	-10.74	34.427	55.205
alpha1	1	-32.218	0	5.216
alpha2	1	41.505	34.311	34.031
Deflection	1	61.868	18.122	7.864
C-axial in	1	203.19	221.82	220.97
C-axial out	1	254.59	221.82	203.29
Uin m/s	1	124.03	289.59	455.15
Uout m/s	1	176.99	303.42	429.84
V1 m/s	1	323.77	364.78	487.89
V2 m/s	1	259.13	268.92	356.26
C1 m/s	1	240.17	221.82	221.89
C2 m/s	1	339.95	268.55	245.31
Reaction	1	0.60803	0.73863	0.82703
Diffusion	1	0.38456	0.33965	0.2986
de Haller	1	0.63877	0.73721	0.7937
Flow coefficient	1	1.6383	0.76598	0.48549
Stage load	1	5.1384	0.94255	0.38156
Stage Temp-rise K	1	39.258	39.258	39.258

	Stage	Hubradii	Midradii	Tipradii
beta1	2	44.776	52.446	59.916
beta2	2	2.009	27.241	50
alpha1	2	2.742	11.984	17.446
alpha2	2	43.977	44.945	46.873
Deflection	2	42.767	25.204	9.9159

C-axial in	2	218.11	212.15	203.43
C-axial out	2	248.13	212.15	182.76
Uin m/s	2	226.85	320.97	415.1
Uout m/s	2	248.13	330.52	412.92
V1 m/s	2	307.25	348.07	405.83
V2 m/s	2	248.28	238.62	284.32
C1 m/s	2	218.36	216.88	213.24
C2 m/s	2	344.81	299.74	267.34
Reaction	2	0.44926	0.6	0.68797
Diffusion	2	0.43885	0.45729	0.37939
de Haller	2	0.71031	0.68555	0.77984
Flow coefficient	2	0.96145	0.66097	0.49009
Stage load	2	1.7776	0.88795	0.53092
Stage Temp-rise K	2	45.258	45.258	45.258

	Stage	Hubradii	Midradii	Tipradii
beta1	3	50.622	56.374	61.686
beta2	3	12.93	34.122	51.766
alpha1	3	6.5513	12.817	17.186
alpha2	3	45.27	46.494	48.377
Deflection	3	37.692	22.252	9.9208
C-axial in	3	202.08	196.95	190.49
C-axial out	3	224.99	196.95	172.61
Uin m/s	3	269.41	340.95	412.49
Uout m/s	3	278.78	346.06	413.33
V1 m/s	3	318.51	355.65	401.62
V2 m/s	3	230.85	237.91	278.91
C1 m/s	3	203.4	201.98	199.39
C2 m/s	3	319.7	286.08	259.86
Reaction	3	0.53541	0.63	0.69312
Diffusion	3	0.49431	0.47296	0.39589
de Haller	3	0.65094	0.66892	0.76638
Flow coefficient	3	0.75006	0.57765	0.4618
Stage load	3	1.268	0.79169	0.54089
Stage Temp-rise K	3	45.258	45.258	45.258

	Stage	Hubradii	Midradii	Tipradii
beta1	4	51.145	57.728	63.452
beta2	4	17.476	38.639	55.698
alpha1	4	16.638	21.913	26.171
alpha2	4	47.237	49.873	53.432
Deflection	4	33.669	19.088	7.754
C-axial in	4	186.71	176.87	166.42
C-axial out	4	207.95	176.87	147.88
Uin m/s	4	287.56	351.22	414.88
Uout m/s	4	290.32	353.22	416.12
V1 m/s	4	297.62	331.25	372.35
V2 m/s	4	218.01	226.43	262.4
C1 m/s	4	194.87	190.64	185.43
C2 m/s	4	306.27	274.43	248.21
Reaction	4	0.51202	0.6	0.66118
Diffusion	4	0.49207	0.46819	0.39644

de Haller	4	0.65771	0.68358	0.79309
Flow coefficient	4	0.64929	0.50357	0.40113
Stage load	4	0.97205	0.65163	0.46701
Stage Temp-rise K	4	39.258	39.258	39.258

Velocity Triangles FAN: First stage on top: Hub-Mean-Tip: red in, black out

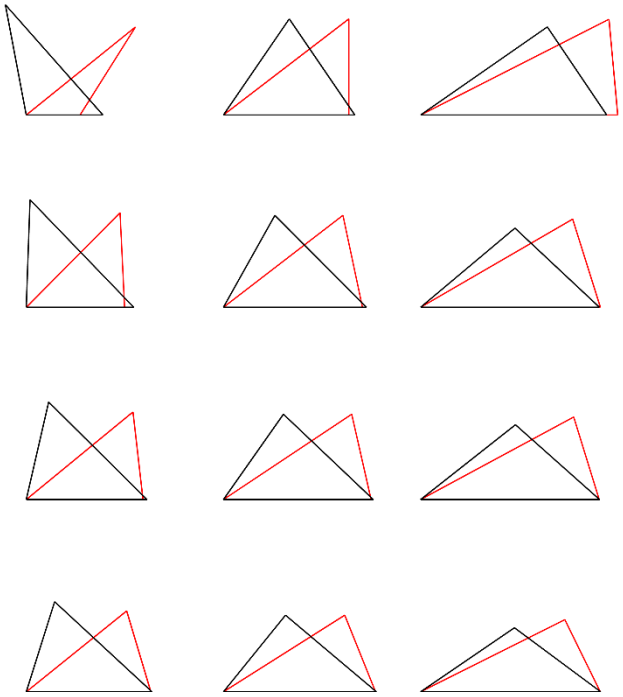

----------Velocity Diagram Compressor-----

IGV angle: 18
First stage Mtip,rel: 1.3421
Average Stage Load: 0.58116
Average Flow coefficient: 0.37835
Average Temp rise: 89.8067

	Stage	Hubradii	Midradii	Tipradii
beta1	1	59.191	67.066	68.265
beta2	1	46.582	51.759	61.289
alpha1	1	11.848	18	20.69
alpha2	1	47.102	47.582	49.396
Deflection	1	12.609	15.306	6.9764
C-axial in	1	228.95	221.24	212.68
C-axial out	1	238.25	221.24	205.13
Uin m/s	1	431.95	522.88	613.8
Uout m/s	1	508.18	560.99	613.8
V1 m/s	1	447	567.76	574.31
V2 m/s	1	346.63	357.44	427.01
C1 m/s	1	233.93	232.63	227.34
C2 m/s	1	350	327.99	315.19
Reaction	1	0.64761	0.69971	0.73964
Diffusion	1	0.38034	0.47122	0.34827
de Haller	1	0.74519	0.62956	0.77085
Flow coefficient	1	0.53003	0.42313	0.34649
Stage load	1	0.96328	0.65739	0.47705
Stage Temp-rise K	1	86.807	86.807	86.807

	Stage	Hubradii	Midradii	Tipradii
beta1	2	65.382	66.703	67.942
beta2	2	54.619	57.398	60.589
alpha1	2	13.717	15.017	16.21
alpha2	2	45.398	45.763	46.162
Deflection	2	10.762	9.3045	7.3534
C-axial in	2	226.76	224.67	222.5
C-axial out	2	231.52	224.67	218.02
Uin m/s	2	550.22	582.01	613.8
Uout m/s	2	560.78	587.29	613.8
V1 m/s	2	544.35	568.06	592.48
V2 m/s	2	399.87	416.98	443.97
C1 m/s	2	233.42	232.61	231.72
C2 m/s	2	329.72	322.04	314.78
Reaction	2	0.73637	0.75	0.76235
Diffusion	2	0.37158	0.36042	0.33478
de Haller	2	0.71946	0.73405	0.76474
Flow coefficient	2	0.41213	0.38602	0.3625
Stage load	2	0.63967	0.5717	0.51401
Stage Temp-rise K	2	91.807	91.807	91.807

	Stage	Hubradii	Midradii	Tipradii
beta1	3	64.154	65.349	66.49
beta2	3	51.159	54.142	57.217
alpha1	3	24.576	25.624	26.638
alpha2	3	51.163	51.895	52.671
Deflection	3	12.995	11.207	9.2734
C-axial in	3	226.09	222.66	219.18
C-axial out	3	231.05	222.66	214.32
Uin m/s	3	570.14	591.97	613.8
Uout m/s	3	573.93	593.87	613.8
V1 m/s	3	518.61	533.83	549.47
V2 m/s	3	368.4	380.1	395.81
C1 m/s	3	248.62	246.94	245.21
C2 m/s	3	368.43	360.8	353.43
Reaction	3	0.65764	0.67	0.68152
Diffusion	3	0.42826	0.41595	0.39781
de Haller	3	0.69513	0.71203	0.73672
Flow coefficient	3	0.39656	0.37613	0.35709
Stage load	3	0.60805	0.56402	0.52461
Stage Temp-rise K	3	91.807	91.807	91.807

	Stage	Hubradii	Midradii	Tipradii
beta1	4	66.495	67.293	68.063
beta2	4	54.411	56.763	59.071
alpha1	4	19.353	20.196	21.006
alpha2	4	50.423	50.924	51.45
Deflection	4	12.084	10.53	8.9918
C-axial in	4	217.95	216.04	214.1
C-axial out	4	222.22	216.04	209.93
Uin m/s	4	577.69	595.75	613.8
Uout m/s	4	579.35	596.58	613.8
V1 m/s	4	546.48	559.66	573.09
V2 m/s	4	381.84	394.16	408.44
C1 m/s	4	231	230.19	229.34
C2 m/s	4	348.79	342.73	336.86
Reaction	4	0.70106	0.71	0.71843
Diffusion	4	0.4306	0.41636	0.39987
de Haller	4	0.68531	0.70429	0.72686
Flow coefficient	4	0.37728	0.36264	0.34881
Stage load	4	0.60446	0.56837	0.53542
Stage Temp-rise K	4	91.807	91.807	91.807

	Stage	Hubradii	Midradii	Tipradii
beta1	5	67.134	67.912	68.663
beta2	5	55.841	58.116	60.285
alpha1	5	23.151	23.952	24.731

alpha2	5	51.863	52.449	53.064
Deflection	5	11.293	9.7957	8.378
C-axial in	5	207.58	205.4	203.2
C-axial out	5	211.7	205.4	199.14
Uin m/s	5	580.98	597.39	613.8
Uout m/s	5	581.61	597.71	613.8
V1 m/s	5	534.2	546.24	558.49
V2 m/s	5	377.03	388.87	401.75
C1 m/s	5	225.76	224.76	223.72
C2 m/s	5	342.8	337.02	331.39
Reaction	5	0.69157	0.7	0.70798
Diffusion	5	0.42568	0.4114	0.39632
de Haller	5	0.69205	0.71191	0.73404
Flow coefficient	5	0.35729	0.34383	0.33106
Stage load	5	0.57551	0.54432	0.51561
Stage Temp-rise K	5	86.807	86.807	86.807

Velocity Triangles Compressor: First stage on top: Hub-Mean-Tip: red in, black out

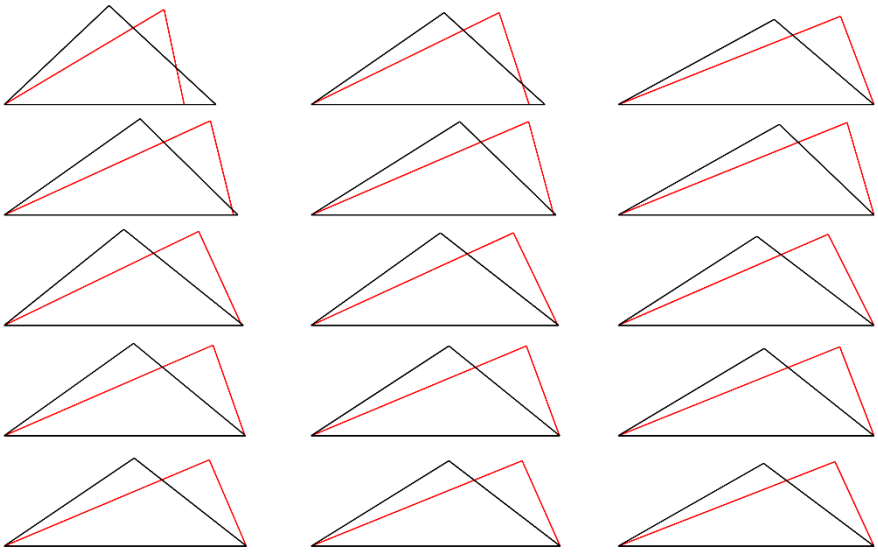

----------Velocity Diagram HPT----------

Avg. Stage load 3.101
Avg. Flow coefficient 0.41135

	Stage	Hubradii	Midradii	Tipradii
beta2	1	58.989	51.748	42.042
beta3	1	66.991	68.206	70.037
alpha2	1	75.772	74.874	73.983
alpha3	1	4.2634	4	3.6162
Deflection	1	8.0023	16.458	27.995
C-axial in	1	259.33	259.33	259.33
U m/s	1	591.35	630.43	669.52
V2 m/s	1	503.36	418.86	349.2
V3 m/s	1	663.47	698.49	759.58
C2 m/s	1	1055.1	993.8	939.85
C3 m/s	1	260.05	259.96	259.85
Relative Mach #	1	0.42712	0.35277	0.2923
Reaction	1	0.19342	0.25351	0.3572
Flow coefficient	1	0.41135	0.41135	0.41135
Stage load	1	3.101	3.101	3.101
Stage Temp-drop K	1	494.16	494.16	494.16
P2/Pchoke < 1	1	0.85975	0.85975	0.85975

Velocity Triangles HPT: First stage on top: Hub-Mean-Tip: red inlet, black exit

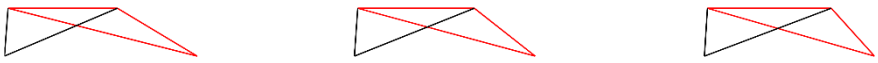

----------Velocity Diagram LPT----------

Avg. Stage load 2.056
Avg. Flow coefficient 0.80783

	Stage	Hubradii	Midradii	Tipradii
beta2	1	21.753	4.1707	-12.257
beta3	1	49.486	52.837	56.013
alpha2	1	57.493	54.309	51.36
alpha3	1	0	0	0
Deflection	1	27.732	48.666	68.27
C-axial in	1	253.6	253.6	253.6
U m/s	1	296.77	334.54	372.31
V2 m/s	1	273.04	254.27	259.51
V3 m/s	1	390.37	419.8	453.66
C2 m/s	1	471.9	434.68	406.13
C3 m/s	1	253.6	253.6	253.6
Relative Mach #	1	0.43013	0.3978	0.40403
Reaction	1	0.35946	0.47236	0.59675
Flow coefficient	1	0.75804	0.75804	0.75804
Stage load	1	2.1106	2.1106	2.1106
Stage Temp-drop K	1	99.661	99.661	99.661
P2/Pchoke < 1	1	0.73794	0.73794	0.73794

	Stage	Hubradii	Midradii	Tipradii
beta2	2	18.955	0.046184	-16.582
beta3	2	45.207	49.383	54.209
alpha2	2	53.485	49.402	45.763
alpha3	2	0	0	0
Deflection	2	26.252	49.337	70.79
C-axial in	2	294.64	294.64	294.64
U m/s	2	296.77	343.55	390.32
V2 m/s	2	311.53	294.64	307.42
V3 m/s	2	418.19	452.59	503.79
C2 m/s	2	495.16	452.77	422.34
C3 m/s	2	294.64	294.64	294.64
Relative Mach #	2	0.47108	0.44216	0.45906
Reaction	2	0.36351	0.49965	0.68916
Flow coefficient	2	0.85763	0.85763	0.85763
Stage load	2	2.0014	2.0014	2.0014
Stage Temp-drop K	2	99.661	99.661	99.661
P2/Pchoke < 1	2	0.73757	0.73757	0.73757

Velocity Triangles LPT: First stage on top: Hub-Mean-Tip: red inlet, black exit

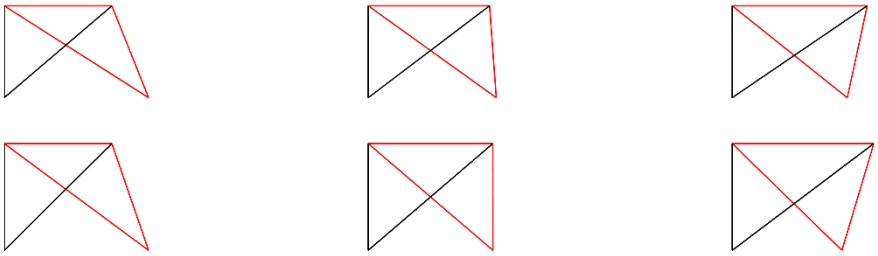

D T-AXI DISK output files

First HPC disc

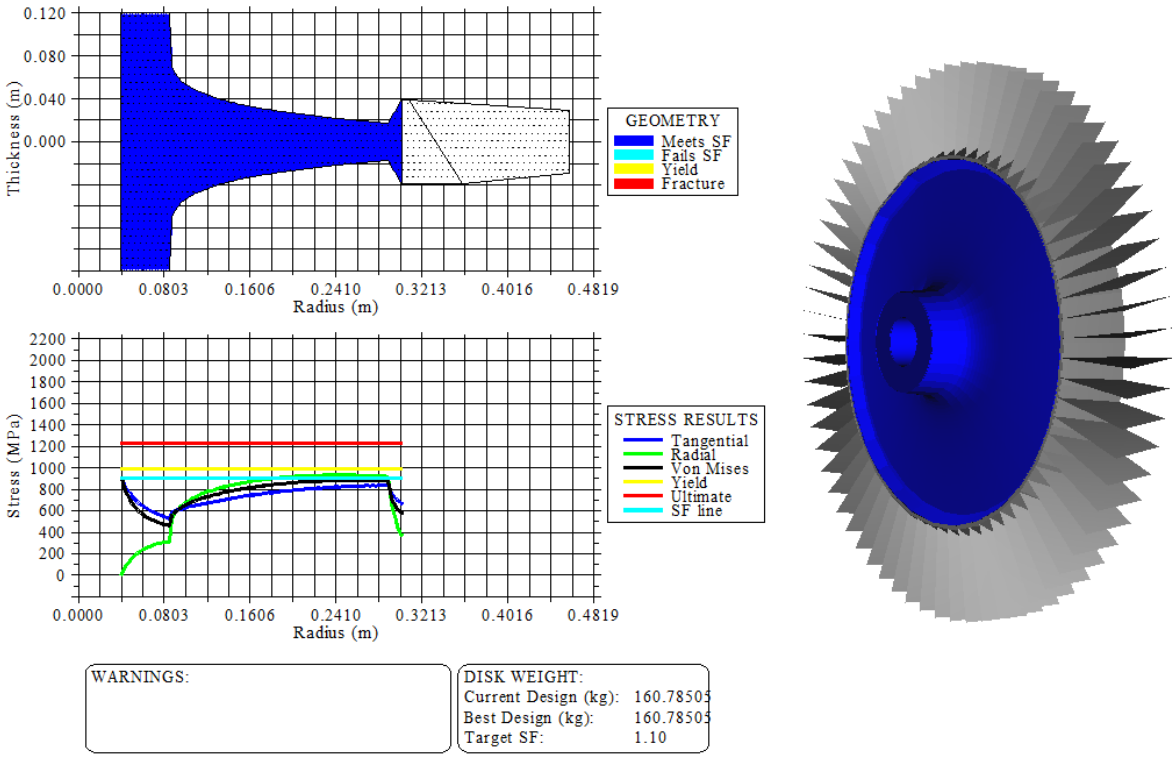

WARNINGS:	DISK WEIGHT:	
	Current Design (kg):	160.78505
	Best Design (kg):	160.78505
	Target SF:	1.10

```
&INPUT_OUTPUT
 C1="*******T-AXI_DISK_INPUT_FILE:_VERSION_2.4*******"
 C2="*******PARAMATERIZATION_TYPE********************"
 TYPE=           2
 C3="*****************PARAMETERS*********************"
 DRQR=  1.00010000169277191E-002
 WWEB=  0.44678959250450134
 DRQB=  0.57624977827072144
 WBOR=  0.23997600376605988
 RBOR=  4.00040000677108765E-002
 DSF=  0.16814558207988739
 PR1=  0.50000000000000000
 PR2=  0.50000000000000000
 PT1=  1.00000000000000000
 PT2=  0.25000000000000000
 PT3=  0.25000000000000000
 S12=  0.50000000000000000
 C4="*****************DISK_MATERIAL*****************"
 MATNAME="INCONEL718.dmat"
 C5="**********DEAD_WEIGHT_SPECIFICATION*************"
 DEAD_WEIGHT_FLAG=           1
 M_B=   1.1856651650167098
 R_CG_B=  0.35306778472642797
 C6="**************ANALYSIS_CONDITIONS***************"
 RPMO=   13500.000000000000
 TADDER=   0.0000000000000000
 RIMT=   150.00000000000000
 TAXIS=   145.00000000000000
 SFACT=   1.1000000000000001
 C7="*****************OTHER_VALUES******************"
 BNUM=   65.000000000000000
 BIRR=  0.30900000000000000
 BERR=  0.35899999999999999
 WRIM=  7.79999999999999999E-002
 BSPN=  0.12500000000000000
 BSHR=           2
 BRHO=   8000.0000000000000
 BTHP=   7.0000000000000000
 RTQB=  0.25000000000000000
 WBOR_MAX=  0.23997599999999999
 RBOR_MIN=  4.00039999999999979E-002
 BFILENAME="none"
 BSCALE=  1.00000000000000000       /
```

Second HPC disc

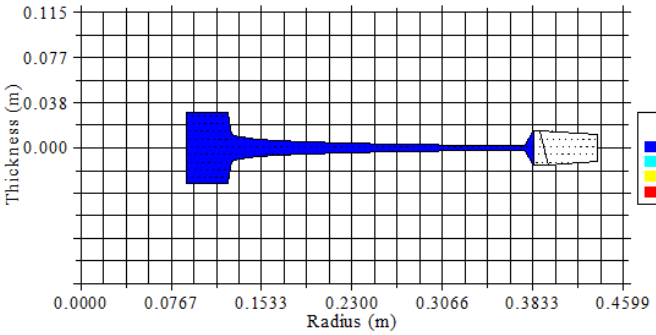

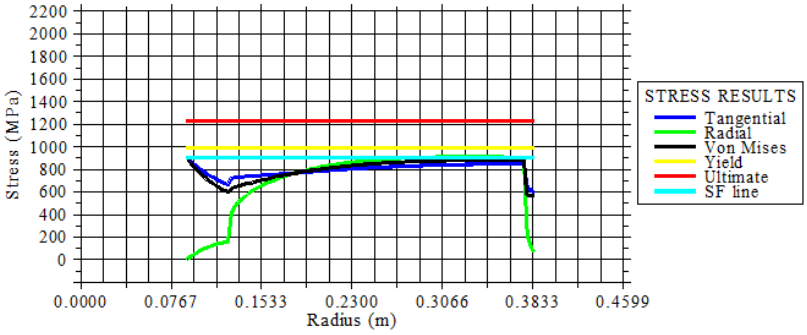

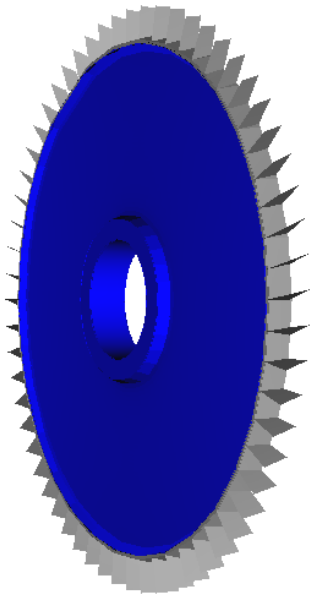

WARNINGS:	DISK WEIGHT:	
	Current Design (kg):	38.28481
	Best Design (kg):	38.05155
	Target SF:	1.10

```
&INPUT_OUTPUT
C1="*******T-AXI_DISK_INPUT_FILE:_VERSION_2.4*******"
C2="*******PARAMATERIZATION_TYPE********************"
TYPE=           2
C3="*****************PARAMETERS*********************"
DRQR=  1.00010000169277191E-002
WWEB=  0.10898753255605698
DRQB=   1.1600420475006104
WBOR=  5.99999986588954926E-002
RBOR=  9.00089964270591736E-002
DSF=  0.10001000016927719
PR1=  0.50000000000000000
PR2=  0.50000000000000000
PT1=  1.00000000000000000
PT2=  0.25000000000000000
PT3=  0.25000000000000000
S12=  0.50000000000000000
C4="*****************DISK_MATERIAL******************"
MATNAME="INCONEL718.dmat"
C5="**********DEAD_WEIGHT_SPECIFICATION*************"
DEAD_WEIGHT_FLAG=           1
M_B=  0.11507518039625086
R_CG_B=  0.39494879717528664
C6="**************ANALYSIS_CONDITIONS***************"
RPMO=   13500.000000000000
TADDER=   0.0000000000000000
RIMT=   150.00000000000000
TAXIS=   145.00000000000000
SFACT=   1.1000000000000001
C7="*****************OTHER_VALUES*******************"
BNUM=   60.000000000000000
BIRR=  0.38900000000000001
BERR=  0.39700000000000002
WRIM=  2.99999999999999989E-002
BSPN=  4.49999999999999983E-002
BSHR=           2
BRHO=   8000.0000000000000
BTHP=   7.0000000000000000
RTQB=  0.20000000000000001
WBOR_MAX=  6.99930000000000135E-002
RBOR_MIN=  9.00089999999999918E-002
BFILENAME="none"
BSCALE=  1.00000000000000000       /
```

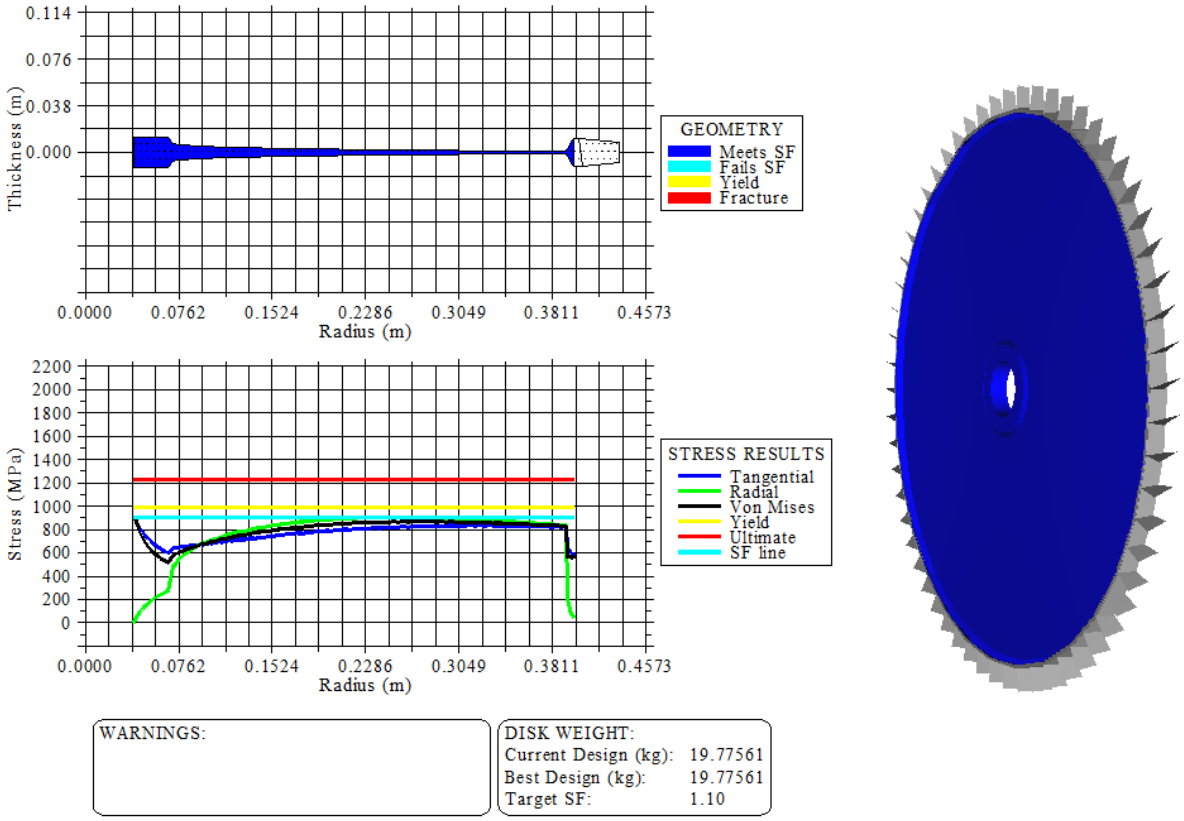
0.114
0.076
0.038
0.000
Thickness (m)
0.0000
0.0762
0.1524
0.2286
0.3049
0.3811
0.4573
Radius (m)
GEOMETRY
Meets SF
Fails SF
Yield
Fracture
2200
2000
1800
1600
1400
1200
1000
800
600
400
200
0
Stress (MPa)
STRESS RESULTS
Tangential
Radial
Von Mises
Yield
Ultimate
SF line
WARNINGS:
DISK WEIGHT:
Current Design (kg): 19.77561
Best Design (kg): 19.77561
Target SF: 1.10

```
&INPUT_OUTPUT
C1="*******T-AXI_DISK_INPUT_FILE:_VERSION_2.4*******"
C2="*******PARAMATERIZATION_TYPE********************"
TYPE=           2
C3="*****************PARAMETERS*********************"
DRQR=  9.99999974737875164E-005
WWEB=  8.00120010972023010E-002
DRQB=   1.2000399827957153
WBOR=  2.49975007027387619E-002
RBOR=  4.00040000677108765E-002
DSF=  0.18009099364280701
PR1=  0.50000000000000000
PR2=  0.50000000000000000
PT1=  1.00000000000000000
PT2=  0.25000000000000000
PT3=  0.25000000000000000
S12=  0.50000000000000000
C4="*****************DISK_MATERIAL******************"
MATNAME="INCONEL718.dmat"
C5="**********DEAD_WEIGHT_SPECIFICATION*************"
DEAD_WEIGHT_FLAG=           1
M_B=  5.81338048435073584E-002
R_CG_B=  0.40494046444841159
C6="**************ANALYSIS_CONDITIONS***************"
RPMO=   13500.000000000000
TADDER=   0.0000000000000000
RIMT=   150.00000000000000
TAXIS=   145.00000000000000
SFACT=   1.1000000000000001
C7="*****************OTHER_VALUES*******************"
BNUM=   60.000000000000000
BIRR=  0.40300000000000002
BERR=  0.40600000000000003
WRIM=  2.29999999999999996E-002
BSPN=  3.09999999999999998E-002
BSHR=           2
BRHO=   8000.0000000000000
BTHP=   7.0000000000000000
RTQB=  0.20000000000000001
WBOR_MAX=  2.99969999999999994E-002
RBOR_MIN=  4.00039999999999979E-002
BFILENAME="none"
BSCALE=  1.00000000000000000       /
```

Fourth HPC disc

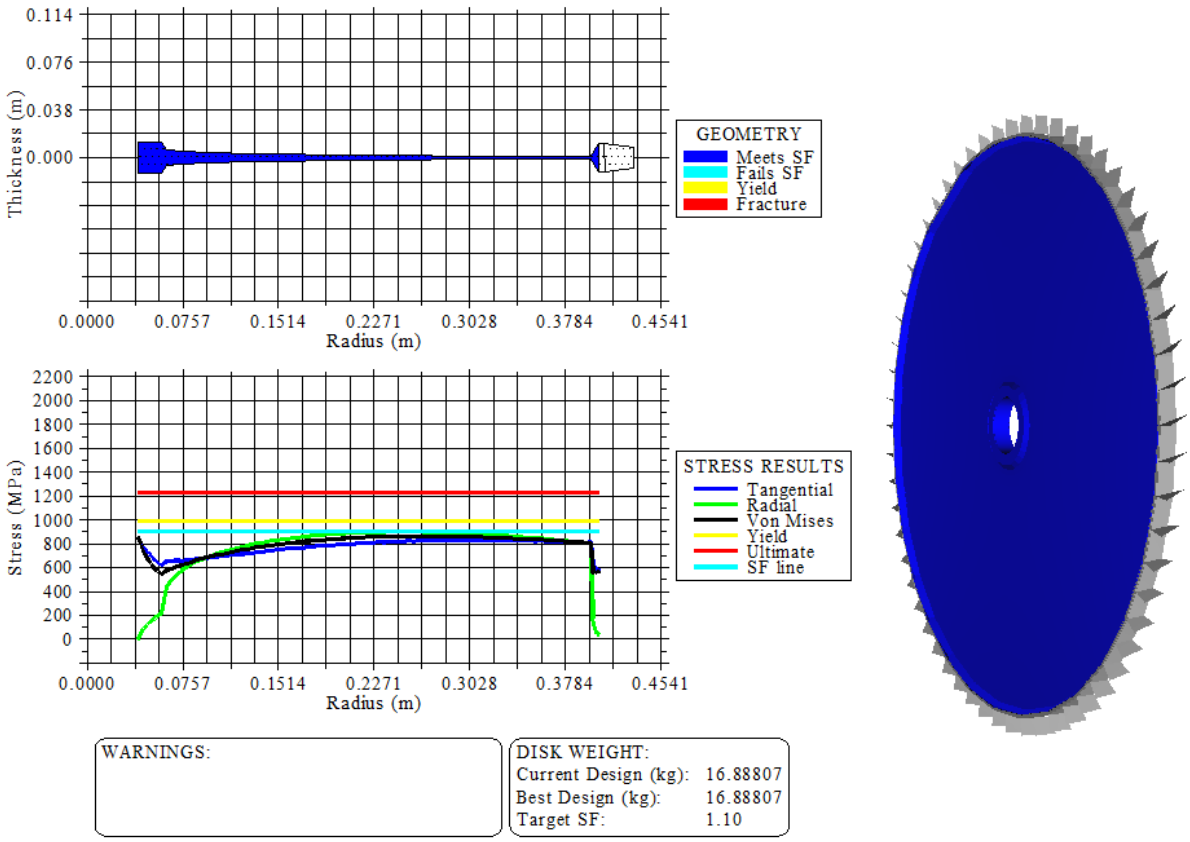

```
&INPUT_OUTPUT
C1="*******T-AXI_DISK_INPUT_FILE:_VERSION_2.4*******"
C2="*******PARAMATERIZATION_TYPE********************"
TYPE=           2
C3="*****************PARAMETERS*********************"
DRQR=  1.00010000169277191E-002
WWEB=  6.81580975651741028E-002
DRQB=  0.86708587408065796
WBOR=  2.46679987758398056E-002
RBOR=  4.00040000677108765E-002
DSF=  0.15354484319686890
PR1=  0.50000000000000000
PR2=  0.50000000000000000
PT1=  1.00000000000000000
PT2=  0.25000000000000000
PT3=  0.25000000000000000
S12=  0.50000000000000000
C4="*****************DISK_MATERIAL*****************"
MATNAME="INCONEL718.dmat"
C5="**********DEAD_WEIGHT_SPECIFICATION*************"
DEAD_WEIGHT_FLAG=           1
M_B=  4.14624665236959580E-002
R_CG_B=  0.40971401261695956
C6="**************ANALYSIS_CONDITIONS***************"
RPMO=   13500.000000000000
TADDER=   0.0000000000000000
RIMT=   150.00000000000000
TAXIS=   145.00000000000000
SFACT=   1.1000000000000001
C7="*****************OTHER_VALUES******************"
BNUM=   60.000000000000000
BIRR=  0.40899999999999997
BERR=  0.40999999999999998
WRIM=  2.19999999999999987E-002
BSPN=  2.29999999999999996E-002
BSHR=           2
BRHO=   8000.0000000000000
BTHP=   7.0000000000000000
RTQB=  0.20000000000000001
WBOR_MAX=  2.49975000000000024E-002
RBOR_MIN=  4.00039999999999979E-002
BFILENAME="none"
BSCALE=  1.00000000000000000       /
```

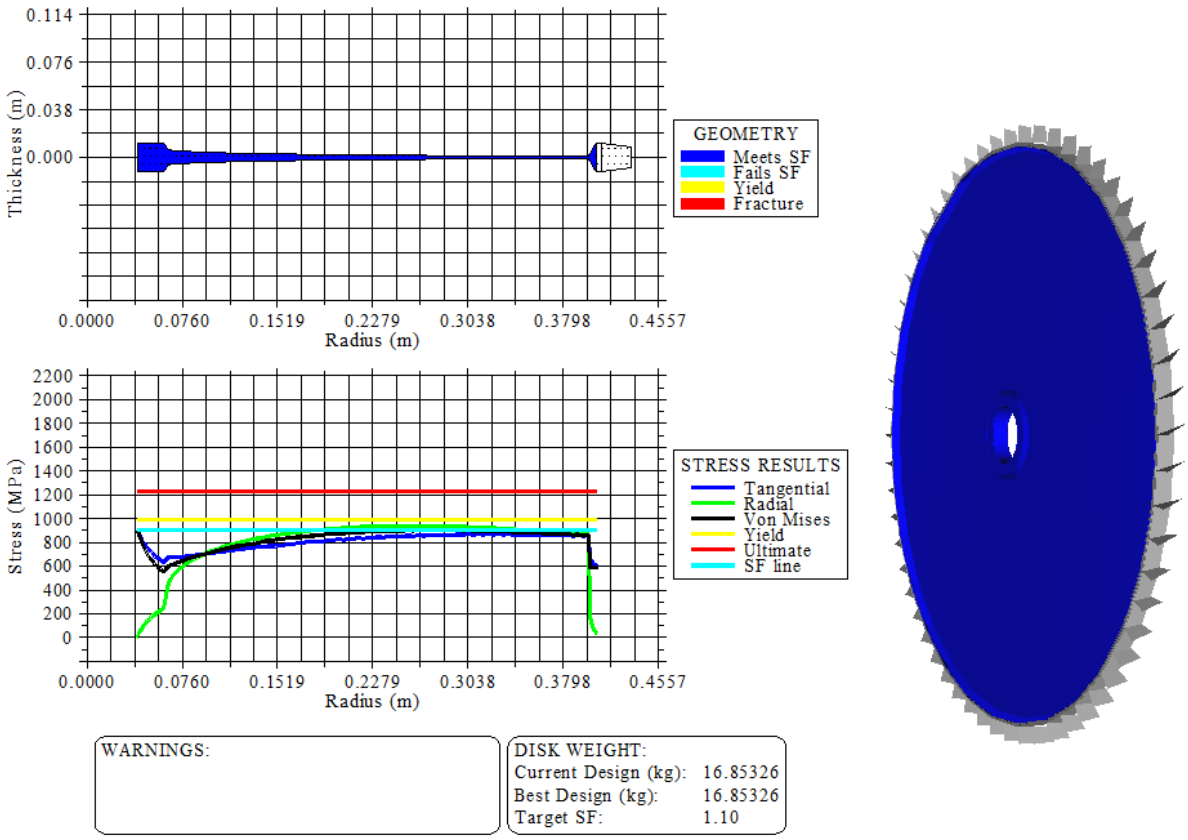
0.114
0.076
0.038
0.000
Thickness (m)
0.0000
0.0760
0.1519
0.2279
0.3038
0.3798
0.4557
Radius (m)
GEOMETRY
Meets SF
Fails SF
Yield
Fracture
2200
2000
1800
1600
1400
1200
1000
800
600
400
200
0
Stress (MPa)
STRESS RESULTS
Tangential
Radial
Von Mises
Yield
Ultimate
SF line
WARNINGS:
DISK WEIGHT:
Current Design (kg): 16.85326
Best Design (kg): 16.85326
Target SF: 1.10

```
&INPUT_OUTPUT
C1="*******T-AXI_DISK_INPUT_FILE:_VERSION_2.4*******"
C2="*******PARAMATERIZATION_TYPE********************"
TYPE=           2
C3="*****************PARAMETERS*********************"
DRQR=  1.00010000169277191E-002
WWEB=  6.48523047566413879E-002
DRQB=  0.90963256359100342
WBOR=  2.29748580604791641E-002
RBOR=  4.00040000677108765E-002
DSF=  0.16116099059581757
PR1=  0.50000000000000000
PR2=  0.50000000000000000
PT1=  1.00000000000000000
PT2=  0.25000000000000000
PT3=  0.25000000000000000
S12=  0.50000000000000000
C4="*****************DISK_MATERIAL*****************"
MATNAME="INCONEL718.dmat"
C5="**********DEAD_WEIGHT_SPECIFICATION*************"
DEAD_WEIGHT_FLAG=           1
M_B=  4.39481341670272668E-002
R_CG_B=  0.41129828749125069
C6="**************ANALYSIS_CONDITIONS***************"
RPMO=   13500.000000000000
TADDER=   0.0000000000000000
RIMT=   150.00000000000000
TAXIS=   145.00000000000000
SFACT=   1.1000000000000001
C7="*****************OTHER_VALUES******************"
BNUM=   60.000000000000000
BIRR=  0.41099999999999998
BERR=  0.41099999999999998
WRIM=  2.29999999999999996E-002
BSPN=  2.29999999999999996E-002
BSHR=           2
BRHO=   8000.0000000000000
BTHP=   7.0000000000000000
RTQB=  0.20000000000000001
WBOR_MAX=  2.39976000000000009E-002
RBOR_MIN=  4.00039999999999979E-002
BFILENAME="none"
BSCALE=  1.00000000000000000       /
```

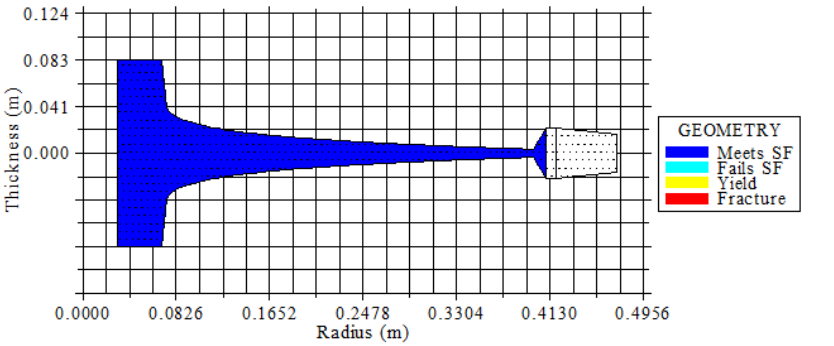

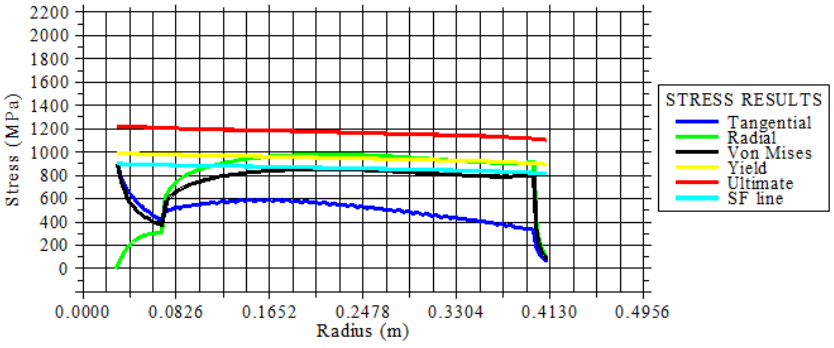

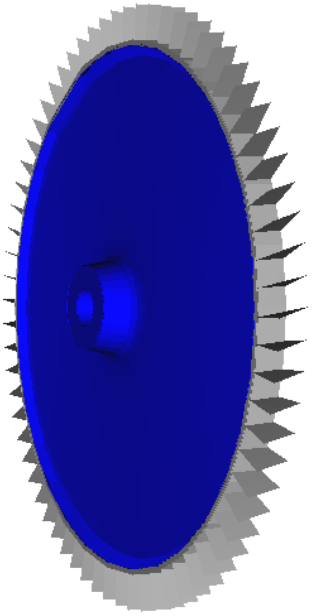

WARNINGS:	DISK WEIGHT:	
	Current Design (kg):	104.34225
	Best Design (kg):	104.34225
	Target SF:	1.10

```
&INPUT_OUTPUT
C1="*******T-AXI_DISK_INPUT_FILE:_VERSION_2.4*******"
C2="*******PARAMATERIZATION_TYPE********************"
TYPE=           2
C3="*****************PARAMETERS*********************"
DRQR=  1.00010000169277191E-002
WWEB=  0.15955232083797455
DRQB=  0.90005499124526978
WBOR=  0.16498349606990814
RBOR=  3.00030000507831573E-002
DSF=  0.14009299874305725
PR1=  0.50000000000000000
PR2=  0.50000000000000000
PT1=  1.00000000000000000
PT2=  0.25000000000000000
PT3=  0.25000000000000000
S12=  0.50000000000000000
C4="*****************DISK_MATERIAL******************"
MATNAME="INCONEL718.dmat"
C5="**********DEAD_WEIGHT_SPECIFICATION*************"
DEAD_WEIGHT_FLAG=           1
M_B=  0.18910831139661863
R_CG_B=  0.42570518476269659
C6="**************ANALYSIS_CONDITIONS***************"
RPMO=   13500.000000000000
TADDER=   0.0000000000000000
RIMT=   600.00000000000000
TAXIS=   145.00000000000000
SFACT=   1.1000000000000001
C7="*****************OTHER_VALUES*******************"
BNUM=   68.000000000000000
BIRR=  0.41799999999999998
BERR=  0.41799999999999998
WRIM=  4.39999999999999974E-002
BSPN=  5.39999999999999994E-002
BSHR=           2
BRHO=   8000.0000000000000
BTHP=   7.0000000000000000
RTQB=  0.14999999999999999
WBOR_MAX=  0.16498350000000001
RBOR_MIN=  3.00029999999999984E-002
BFILENAME="none"
BSCALE=  1.00000000000000000       /
```